Effective interactions for nucleon-nucleus scattering above 300 MeV

L. Ray
Department of Physics, The University of Texas at Austin, Austin, Texas 78712
(Received 25 October 1989)

A nonrelativistic nucleon-nucleon (*NN*) coupled channels isobar model is used to calculate nuclear medium corrections to the first-order Watson optical potential for nucleon-nucleus scattering. The *NN* interaction includes π, 2π, ρ, η, and ω exchange for the pure nucleonic sector, one-pion exchange for nucleon-isobar coupling, and phenomenological short-range interactions for both the diagonal and coupling terms. Good fits to *NN* elastic phase shifts from 0–1 GeV have been obtained with this model. The specific nuclear medium effects studied here include Pauli blocking of intermediate nucleon scattering states and off-shell binding energy shifts. On-momentum-shell matrix elements of the density dependent, effective *NN* t matrix are used to calculate the local proton-nucleus optical potential assuming the local density approximation. The model is applied to proton elastic scattering from ^{16}O, ^{40}Ca, ^{48}Ca, and ^{208}Pb at 320, 400, 500, 650, and 800 MeV and the predictions are compared with available data. In general, the medium modifications significantly affect the nonrelativistic predictions, even at 800 MeV, and bring about a substantial, overall improvement in the description of differential cross section and spin observable data. The improvements occur for each case and at all angles studied, but the agreement is most successful for forward angle differential cross sections and for spin observable data from 1 to 3 fm^{-1}. Deficiencies remain in the density dependent, nonrelativistic predictions for the forward angle spin observables where relativistic models are quite successful. The relation of this work to other nonrelativistic models which include nuclear medium corrections, off-shell effects, and full-folding contributions is also discussed.

I. INTRODUCTION

A principal deficiency in all preceding efforts to understand nucleon-nucleus scattering phenomenon above 400 MeV in terms of nonrelativistic (NR) multiple scattering theories is the reliance upon the impulse approximation (IA).[1] The basic assumption underlying the IA is that effects of the nuclear medium on the propagation of the *NN* system in intermediate scattering states are negligible. Given the validity of this assumption the complicated nucleon-nucleon (*NN*) effective interaction of multiple scattering theory can be accurately represented by just the free *NN* elastic scattering amplitudes. Theoretical predictions based on the IA are, however, not in satisfactory agreement with proton-nucleus (pA) data, particularly for spin observables at energies around 500 MeV.[2–4]

At lower energies ($\leq$400 MeV) NR theoretical predictions including nuclear medium modifications demonstrate considerably improved agreement with experiment.[5–12] Better descriptions of proton-nucleus elastic scattering data for energies at and below 500 MeV also result when *NN* off-shell dependences and full-folding of the first-order optical potential are included.[13–15] Quantitative fits to pA scattering data for energies less than 400 MeV often result in these applications.

The implication of the studies of medium modifications at lower energies and of off-shell and full-folding effects is that such corrections might also be significant at higher energies. Two examples of this have been reported. First, at 500 MeV surprisingly large off-shell effects were demonstrated for proton-nucleus elastic scattering[15] using *NN* t matrices computed from the extended Bonn potential.[16] Second, studies[17,18] from 50 to 450 MeV of zero degree charge exchange cross sections indicate significant reduction of the Fermi strength in the nuclear medium from that predicted by the IA.

In recent years it has been shown that scattering models which include relativistic dynamics provide quantitative descriptions of intermediate energy proton-nucleus elastic scattering data, particularly spin observables.[4,19–24] In these models a local, Lorentz invariant form for the *NN* amplitudes was assumed,[25] scalar and vector nuclear densities were taken from relativistic mean field theory,[26] and the Dirac equation was used to describe the motion of the projectile. These calculations provide, at present, the best overall theoretical description of proton-nucleus scattering data for energies greater than about 400 MeV. Fairly successful extensions to lower energies have also been presented.[21–23]

The success of the relativistic scattering models and the contrasting failure of the NRIA predictions have brought into question the value of an NR many-body Schrödinger equation interpretation of nuclear physics. However, before such conclusions can be firmly drawn the systematic corrections in both theoretical approaches must be studied in greater detail.

It is therefore both timely and important to proceed with improvements in nonrelativistic scattering models. This is done both to more fully understand the possible shortcomings of nonrelativistic theories of nuclear systems and to determine the general importance of many-body corrections to NRIA models.

The focus of the present work is on medium

modifications in NR models at energies above 300 MeV. Pauli blocking and binding energy corrections were estimated assuming the nucleon-isobar coupled channels model of Ref. 27, the infinite nuclear matter limit for the medium modified two-body propagator, and the local density approximation (LDA).[5] The free space NN interaction was used without modification in the nuclear medium.

This work addresses the following questions: (1) How important are Pauli blocking and nuclear binding corrections to the IA amplitudes above 400 MeV? (2) How do these corrections affect the NR predictions for proton-nucleus elastic scattering observables? (3) How much of the success of the relativistic models can be accomplished by improving the applications of the nonrelativistic theories? (4) What deficiencies remain in the nonrelativistic descriptions of the data which relativistic effects might help explain? (5) What is the role of the $\Delta(1232$ MeV) resonance in determining the proton-nucleus scattering dynamics over this range of energies?

In Sec. II the NN-isobar coupled channels model is summarized and updated, the method of calculating the NN effective interaction t matrices is explained, and the ingredients in the proton-nucleus elastic scattering calculations are discussed. The density dependence of the effective NN interactions and proton-nucleus elastic scattering predictions are shown and discussed in Sec. III. Further discussion and the conclusions are given in Sec. IV.

II. THEORETICAL MODEL

A. Nucleon-nucleon interaction

Calculations of Pauli blocking and intermediate binding energy corrections at medium energies require realistic off-shell dependences. This necessitates the use of an NN interaction model which is applicable at energies above pion production threshold. The results presented here were consequently based on the nonrelativistic NN coupled channels isobar model of Ref. 27. This model uses a meson exchange interaction together with nucleon-isobar [$\Delta(1232$ MeV) and $N^*(1440$ MeV)] coupling and short-range phenomenology to describe the $J \leq 6$, $T=0$ and 1 NN scattering states from 0 to 1000 MeV.[28–30]

In Ref. 27 the S-matrix parameters of the model were erroneously fitted to the K-matrix parameters from the phase shift analysis.[31] Below inelastic threshold the two representations are equivalent; however, when inelasticities occur the S- and K-matrix parameters can be different. For energies up to 1 GeV all of the phase shifts and mixing angles are very nearly the same in the two parametrizations and are thus not affected. However, at the highest energies several of the larger $T=1$ inelasticities were sufficiently different to require new fits. The affected $T=1$ partial wave channels include $^1D_2$, $^1G_4$, $^3P_0$, $^3F_3$, and $^3P_2$-$^3F_2$. In addition Gonzalez and Lomon[32] recently reported new fits to four of these same $T=1$ partial wave channels using new coupling schemes and transition potentials. These five $T=1$ partial wave channels were therefore refitted to the WI84 S-matrix parameters[31] using, in general, the new couplings of Ref. 32. The new values of the potentials for these five partial wave channels are given in Table I using the parameters and notation of Ref. 27.

The new fits to the phase shifts, mixing angles, and inelasticities are as good as or better than the results shown in Ref. 27. The spin-independent and single spin-flip on-shell isoscalar amplitudes [i.e., $a(q)$ and $c(q)$ of Ref. 4] of the model are also in good agreement with those of the phase shift analysis (PSA).[31] These two amplitudes are the primary ones needed in optical potentials for spin-zero targets (see Sec. II D). Over the energy and momentum transfer ranges considered here the imaginary (dominant) parts of $a(q)$ and $c(q)$ from the model and the PSA agree to $\lesssim 5\%$; the real (weaker) parts agree to about 5–15 % as shown in Figs. 1–4.

B. Nucleon-nucleon effective t-matrix

The first-order NR optical potential in the Watson multiple scattering formalism[33] is given by

$$\tilde{U}^{(1)}_{\rm opt}(\mathbf{K},\mathbf{K}',E)=(2\pi)^{-3}\sum_{j=1}^{A}\int d^3p\,\psi_j^*\left[\mathbf{p}+\frac{\mathbf{q}}{2}-\frac{\mathbf{k}_a}{A}\right]\times\left\langle\mathbf{K}';\mathbf{p}+\frac{\mathbf{q}}{2}-\frac{\mathbf{k}_a}{A}\left|t^W(E-H_A)\right|\mathbf{K};\mathbf{p}-\frac{\mathbf{q}}{2}-\frac{\mathbf{k}_a}{A}\right\rangle\psi_j\left[\mathbf{p}-\frac{\mathbf{q}}{2}-\frac{\mathbf{k}_a}{A}\right], \quad (1)$$

where ψ_j are single particle wave functions for the $j=1,2,\ldots,A$ occupied states in the target and $\langle t^W\rangle$ is the fully off-shell matrix element of the NN effective interaction operator in the Watson formalism in the projectile-nucleus center-of-momentum (COM) system. The initial and final wave vectors are given by $\mathbf{K}$ and $\mathbf{K}'$, respectively; E is the energy in the incident channel; H_A is the target nucleus Hamiltonian, $\mathbf{q}=\mathbf{K}-\mathbf{K}'$, and $\mathbf{k}_a=(\mathbf{K}+\mathbf{K}')/2$. The optimally factorized first-order optical potential[25] is obtained by fixing $\langle t^W\rangle$ at its $p=0$ value which corresponds to Breit frame kinematics. Use of just the on-shell part of $\langle t^W\rangle$ results in the usual first-order, local optical potential which has been used extensively in analyses of data.[2,4,34–36]

The Watson NN t matrix is defined by[33,37]

$$t^W=v+vGQt^W, \quad (2)$$

where v represents the NN interaction (assumed to be the

free space NN interaction), Q is a projection operator which restricts intermediate scattering states to the set of physical, antisymmetric excited states of the target nucleus, and the propagator G is given by

$$G=(E-H_0-H_A+i\varepsilon)^{-1}\,, \tag{3}$$

where H_0 is the kinetic energy operator for the projectile-nucleus relative motion. Notice that the energy denominator of the Green's function includes interaction potentials for the constituent nucleons through the target Hamiltonian H_A but does not contain such terms for the projectile as is the case for the G matrix in Brueckner theory.[38]

The Watson t matrix is in general a complicated $(A+1)$-body operator (where A is the number of constituent target nucleons) and exact evaluation of it remains a very formidable task. In this work the projected propagator GQ (or Q/e) for finite nuclei was replaced by that corresponding to two interacting nucleons in infinite nuclear matter[5,39] with Fermi momentum k_F where NN, $N\Delta$, and NN^* channels were distinguished. In this limit the projection operator Q becomes the usual Pauli block-

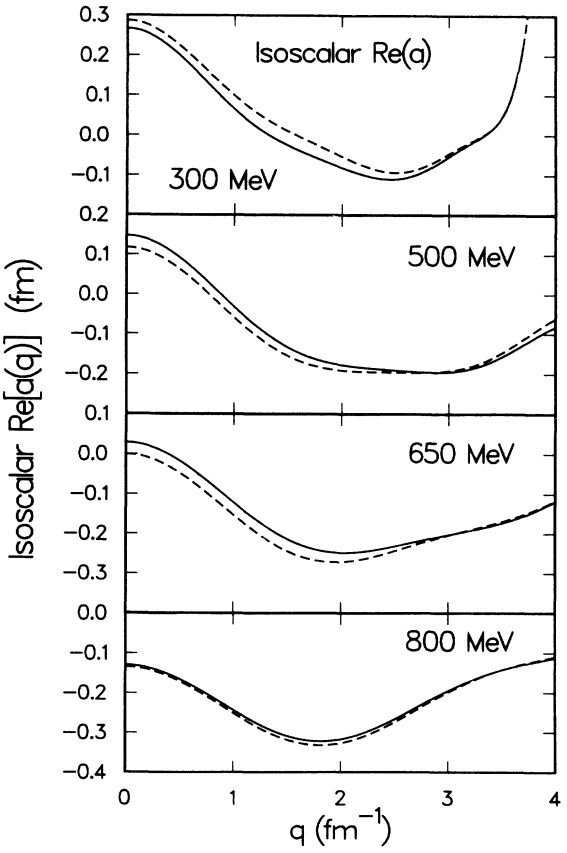

FIG. 1. Model calculations (dashed curves) of the real part of the spin-independent, isoscalar, free NN scattering amplitude at 300, 500, 650, and 800 MeV in comparison with the results of the WI84 phase shift analysis in Ref. 31 (solid curves). For purposes of comparison both sets of amplitudes include just the partial waves through $J=6$ which are the ones obtained in the PSA.

TABLE I. Potential model parameters for the revised $T=1$ partial waves, using the parameter notation of Ref. 27.

NN	$N\Delta_1$	$N\Delta_2$	$V_{NN\text{-}NN}$ type[a]	NN-NN	(V^{1Y},r^{1Y}) (MeV fm,fm) NN-$N\Delta_1$	NN-$N\Delta_2$	$V^1_{N\Delta}$ (MeV)	η_2	$V^3_{N\Delta}$ (MeV)	η_4	$V^5_{N\Delta}$ (MeV)	
$^1D_2$	$^5S_2$	$^5D_2$	FL	(8 500,0.23)	(450,0.715)	(250,0.715)	0.0	1.0	0.0		−13.52	[NN-$N\Delta(S)$]
							0.0	1.0	0.0		16.23	[NN-$N\Delta(D)$]
$^1G_4$	$^5D_4$		FL	(200,0.45)	(0.0)		500.0	2.5	0.0		0.0	
$^3P_0$	$^3P_0$		FL	(95 000,0.15)	(0.0)		20.24	1.0	−130.0	2.0	−10.11	
$^3F_3$	$^5P_3$		FL	(750,0.36)	(0.0)		0.0	1.0	−70.0	2.0	−17.8	
					(V^{1G},r^{1G}) (MeV,fm)							
NN_-	NN_+	$N\Delta$		$NN_-\leftrightarrow NN_-$	$NN_-\leftrightarrow NN_+$	$NN_-\leftrightarrow N\Delta$						
$^3P_2$	$^3F_2$	$^3P_2$	RSC	(650,0.8)	(200,0.8)	(−650,0.8)	0.0	1.0	0.0	2.0	−9.38	($NN_-\leftrightarrow N\Delta$)
							0.0	1.0	200.0	2.0	−10.51	($NN_+\leftrightarrow N\Delta$)

[a]FL means the Feshbach-Lomon interaction for $r\geq r_0=0.735$ fm (see Ref. 28); RSC means the Reid soft core potential for all values of r (see Ref. 30). All other terms not listed are zero.

ing factor.[5] The angle averaged values for Q are given in Appendix A where relativistic kinematics were assumed. Angle averaging of the Pauli blocking operator in infinite nuclear matter has been shown to be a very accurate approximation.[40] The energy denominator e was also evaluated in the infinite nuclear matter limit for each nucleon-isobar channel. The explicit form is given in Appendix B.

In a similar notation the free scattering NN t matrix is given by

$$t = v + vgt \ , \tag{4}$$

where

$$g = (E_0 - H_0 + i\varepsilon)^{-1} \ ,$$

and E_0 is the NN kinetic energy corresponding to the proton-nucleus elastic scattering channel. The Watson and free NN t matrices can be related by eliminating dependence on v, the result being

$$t^W = t + t(GQ - g)t^W \ . \tag{5}$$

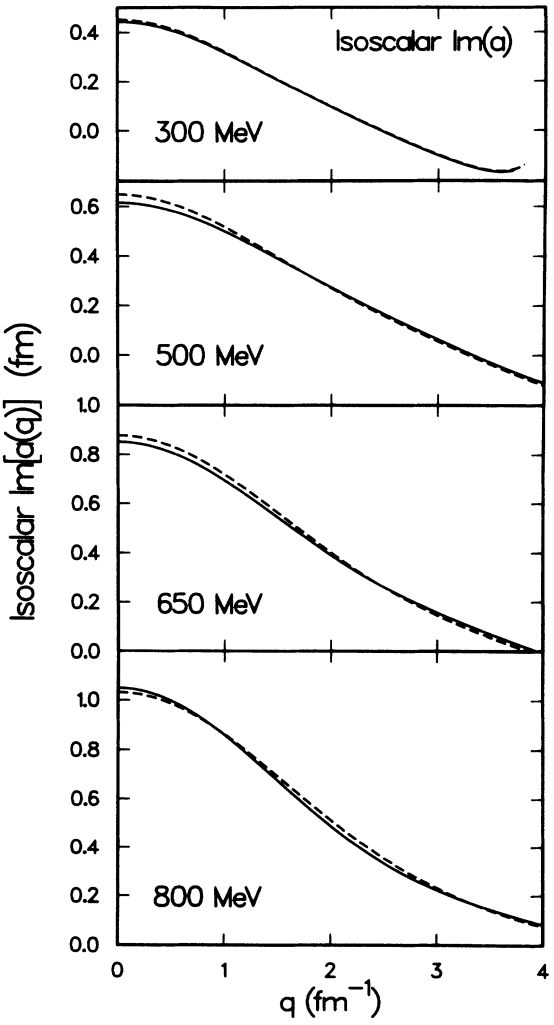

FIG. 2. Same as Fig. 1, except for the imaginary part of the spin-independent, isoscalar scattering amplitude.

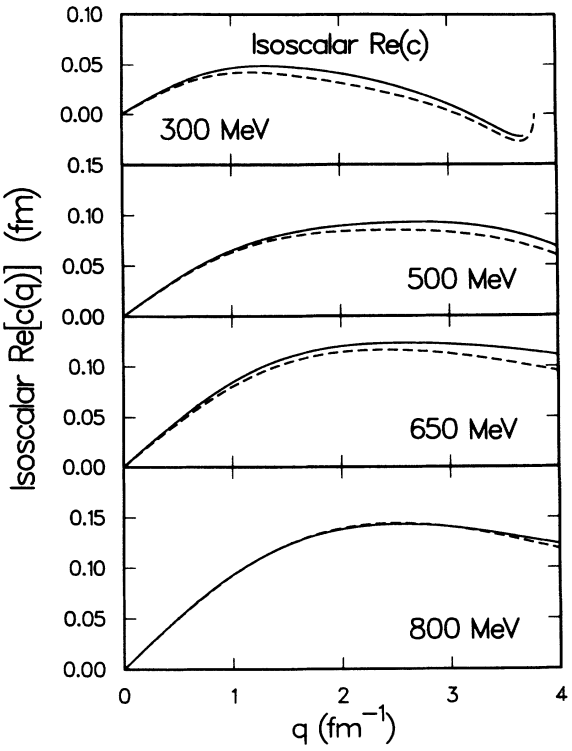

FIG. 3. Same as Fig. 1, except for the real part of the single spin-flip, isoscalar scattering amplitude.

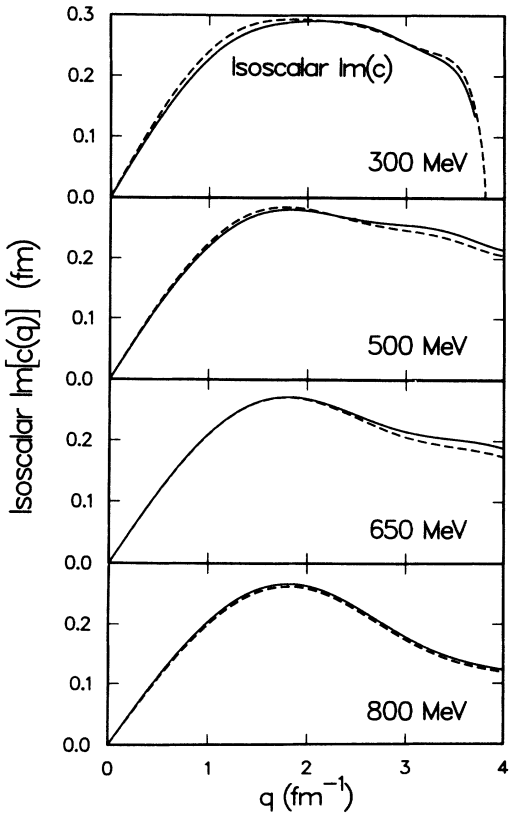

FIG. 4. Same as Fig. 1, except for the imaginary part of the single spin-flip, isoscalar scattering amplitude.

Thus the corrections due to Q and H_A are just contained in the second term on the right-hand side (RHS) of Eq. (5). In the calculations that follow the *NN* coupled channels isobar model is used to estimate just this second term.

The $\langle t(GQ-g)t^W\rangle$ correction is expected to be fairly small compared with $\langle t\rangle$ at intermediate energies. Therefore in this work the medium corrections [second term, RHS of Eq. (5)] were estimated using a local, factorized optical potential form.[41] Several authors[14,15] recently evaluated the fully off-shell, full-folding optical potential corresponding to $\langle t\rangle$ using the Bonn[16] and Paris[42] *NN* interactions and found important effects at intermediate energies. The medium corrections evaluated here should be included *in addition* to these off-shell and full-folding corrections as indicated in Eq. (5). Fermi motion effects can be included by evaluating Eq. (1) and were incorporated in the results of Ref. 14 but were not applied to the second term in Eq. (5) since this would amount to a small "correction to a correction."

The evaluation of the Watson t matrix was facilitated by introducing a wave function ψ defined by

$$t^W\phi = v\psi \ , \tag{6}$$

where ϕ is an *NN* plane wave. The wave function ψ was obtained by solving the integral equation

$$\psi = \phi + GQv\psi \ , \tag{7}$$

in coordinate space using standard partial wave expansion techniques.[5,43] The radial potential was obtained from the quantities given in Table I and the tables of Ref. 27 using the parametrizations given therein. The projected Green's function in coordinate space is given by[5]

$$G(\mathbf{r},\mathbf{r}') = (2\pi)^{-3}\sum_\gamma \int d^3k'_\gamma \langle \mathbf{r}|\mathbf{k}'_\gamma\rangle|\xi_\gamma\rangle \times \left[\frac{Q}{e}\right]_{\gamma,k'_\gamma}\langle\xi_\gamma|\langle\mathbf{k}'_\gamma|\mathbf{r}'\rangle \ , \tag{8}$$

where the intrinsic state of the two particles is denoted by $|\xi_\gamma\rangle$, subscript γ is the label for the intrinsic channel (i.e., *NN*, $N\Delta$, and NN^*), $\mathbf{k}'_\gamma$ is the two-body COM intermediate momentum for channel γ, and $[Q]_{\gamma,k'_\gamma}$ and $[e]_{\gamma,k'_\gamma}$ are given in Appendixes A and B, respectively. For virtual isobar channels and for isobar channels with finite widths[27] the singularity in the integrand of Eq. (8) is removed and the integration was carried out by ordinary quadrature.

Matrix elements of t^W in the *NN* COM system were obtained using Eq. (6). Relating this to the scattering amplitude we get

$$f(\mathbf{k},\mathbf{k}') = -\frac{\mu_{NN}}{2\pi\hbar^2}\langle\phi_{\mathbf{k}'}|v|\psi_{\mathbf{k}}\rangle \ , \tag{9}$$

where subscripts $\mathbf{k}$ and $\mathbf{k}'$ denote the initial and final relative momentum vectors in the *NN* COM system, respectively, and μ_{NN} is the *NN* reduced mass. The on-shell scattering amplitude is often expressed in Wolfenstein form,[44]

$$f = a + c(\sigma_{1n}+\sigma_{2n}) + m\sigma_{1n}\sigma_{2n} + (g+h)\sigma_{1Q}\sigma_{2Q} + (g-h)\sigma_{1q}\sigma_{2q} \ , \tag{10}$$

where $\{a,c,m,g,h\}$ are complex functions of momentum transfer, subscripts 1 and 2 refer to the two nucleons, $\sigma_{1x}\equiv\boldsymbol{\sigma}_1\cdot\hat{\mathbf{x}}$, and the coordinate system is defined by $\hat{\mathbf{n}}=(\mathbf{k}\times\mathbf{k}')/|\mathbf{k}\times\mathbf{k}'|$, $\hat{\mathbf{Q}}=(\mathbf{k}+\mathbf{k}')/|\mathbf{k}+\mathbf{k}'|$, and $\hat{\mathbf{q}}=(\mathbf{k}-\mathbf{k}')/|\mathbf{k}-\mathbf{k}'|$. The scattering amplitude may also be represented in terms of spin and isospin dependences according to the following form:

$$\begin{aligned} f = {} & f_0 + f_\tau(\boldsymbol{\tau}_1\cdot\boldsymbol{\tau}_2) + f_\sigma(\boldsymbol{\sigma}_1\cdot\boldsymbol{\sigma}_2) + f_{\sigma\tau}(\boldsymbol{\sigma}_1\cdot\boldsymbol{\sigma}_2)(\boldsymbol{\tau}_1\cdot\boldsymbol{\tau}_2) \\ & + f_0^{LS}(\boldsymbol{\sigma}_1+\boldsymbol{\sigma}_2)\cdot\hat{\mathbf{n}} + f_\tau^{LS}(\boldsymbol{\sigma}_1+\boldsymbol{\sigma}_2)\cdot\hat{\mathbf{n}}(\boldsymbol{\tau}_1\cdot\boldsymbol{\tau}_2) \\ & + f_0^T S_{12}(\hat{\mathbf{q}}) + f_\tau^T S_{12}(\hat{\mathbf{q}})(\boldsymbol{\tau}_1\cdot\boldsymbol{\tau}_2) + f_0^{T'} S_{12}(\hat{\mathbf{Q}}) \\ & + f_\tau^{T'} S_{12}(\hat{\mathbf{Q}})(\boldsymbol{\tau}_1\cdot\boldsymbol{\tau}_2) \ . \end{aligned} \tag{11}$$

In Eq. (11) τ is the nucleon isospin operator and the tensor operators are given by $S_{12}(\hat{\mathbf{x}})\equiv 3\sigma_{1x}\sigma_{2x}-\boldsymbol{\sigma}_1\cdot\boldsymbol{\sigma}_2$. For elastic scattering from spin 0 targets the important amplitudes are a and c in Eq. (10) or f_0 and f_0^{LS} in Eq. (11).

The remaining steps in the calculation of the effective interaction are as follows: (1) For each value of k_F the on-momentum-shell amplitudes in the *NN* COM system in Eq. (9) were relativistically transformed into t matrices in the pA COM Breit kinematic frame[25,41] using the Wigner rotation matrix[25] as in Eq. (35) of Ref. 4. For the on-momentum-shell matrix element, values of $\mathbf{k}$ and $\mathbf{k}'$ were assumed which correspond to elastic scattering at the incident beam momentum. The resulting on-momentum-shell matrix elements are denoted by $\langle t^W(k_F)\rangle_{\text{Model}}$. The density dependence is therefore generated by the quantity $\langle t^W(k_F)-t^W(k_F=0)\rangle_{\text{Model}}$ which corresponds to the model estimate of the second term on the RHS of Eq. (5) evaluated in the pA COM Breit frame. (2) The leading term on the RHS of Eq. (5) was evaluated using the actual *NN* scattering amplitudes from phase shift analysis (SP82 solution).[31] The on-shell t-matrix element in the pA COM Breit frame, $\langle t\rangle_{\text{Arndt}}$, was obtained by the same relativistic transformation described previously.[4,25,41] (3) The final, estimated density dependent on-momentum-shell t matrix, $\langle t^W(k_F)\rangle_{\text{Final}}$, was obtained from the definition

$$\langle t^W(k_F)\rangle_{\text{Final}} \equiv \langle t\rangle_{\text{Arndt}} + \langle t^W(k_F)-t^W(k_F=0)\rangle_{\text{Model}} \ , \tag{12}$$

which constitutes our approximate value for $\langle t^W\rangle$ in Eq. (5). In addition to the Fermi momentum k_F this quantity is dependent on laboratory kinetic energy T_L and the momentum transfer q.

Calculation of the local optical potential using $\langle t^W(k_F)\rangle_{\text{Final}}$ rather than $\langle t^W(k_F)\rangle_{\text{Model}}$ has the following advantages: (1) The *NN* model, although quite accurate in its reproduction of the on-shell *NN* phenomenology (see Figs. 1–4), is only used to estimate a small correction [second term, RHS of Eq. (5)]. It does not have to be relied upon for the dominant piece [first term, RHS of Eq. (5)]. (2) *NN* COM energy shifts,[4,25] corresponding to optimal factorization prescriptions, are readily included

in $\langle t \rangle_{\text{Arndt}}$ (Ref. 41) but are computationally time consuming to include in $\langle t^W(k_F) \rangle_{\text{Model}}$. Finally, it should be noted that the use of a rescaling prescription analogous to Eq. (12) in calculations requiring fully off-shell matrix elements is problematic. This is due to the difficulty in specifying a completely satisfactory off-shell extrapolation of the empirical NN on-shell t matrix. This limitation does not invalidate the present estimate of medium effects, however.

C. Intermediate binding potential

The energy denominator in Eq. (8) (see Appendix B) contains an intermediate binding potential U which acts on the target nucleon. This potential was assumed to have the velocity dependent form $U(\kappa^2)=A+B\kappa^2$, where κ denotes the particle momentum in intermediate states in the rest frame of the nuclear medium (i.e., the laboratory system). A more general form which is often used, $U(\kappa^2)=A+B\kappa^2+C\kappa^4$ (Ref. 5), resulted in a spurious pole at higher momentum when realistic parameters A, B, and C were chosen. More appropriate forms (e.g., logarithmic model), which better describe the energy dependence of the real, central proton-nucleus optical potential,[45] lead to a complicated dependence of the position of the scattering pole on the intermediate momentum vector. For this study the simple quadratic form will suffice; the adequacy of this model for $U(\kappa^2)$ was tested by studying parameter sensitivities (see Sec. III D).

For the target nucleon in its initial state the parameter $A_{\alpha,1}$ (see Appendix B) was assumed to be -50 MeV (for NN channels at full density). Parameters $A_{\alpha,2}$ and B_α for the NN channels were chosen to fit the interior well depths of the Schrödinger equivalent real, central optical potentials from Dirac phenomenological fits to $p+{}^{40}$Ca elastic scattering data.[45] For a given incident proton laboratory momentum, K_{lab}, the binding potential parameters were chosen to fit the empirical potential strengths near $K_{\text{lab}}/2$. The reason is due to the fact that the dominant portion of the integral over NN COM intermediate momentum in the Green's function lies near the scattering pole. For such values $|K'_{\alpha,2}|$, the intermediate momentum of the target nucleon in the laboratory system (see Appendix B), varies from approximately 0 to K_{lab} with an average value of $K_{\text{lab}}/2$. Sensitivity studies (see Sec. III D) of the final NN effective amplitudes and pA observables to variations of $A_{\alpha,2}$ and B_α demonstrated that this is the sensitive region of momentum space and that the quadratic form fitted in this way was adequate.

The real, central potential strengths at $r=0$ from Dirac phenomenology for $p+{}^{40}$Ca are shown in Fig. 5 in comparison with three of the models for $U(\kappa^2)$ assumed in this work. The binding energy parameters are listed in Table II. The potential was assumed to be proportional to the nuclear matter density or to k_F^3 where k_F is the Fermi momentum.

Very little is known about the Δ-nucleus or N^*-nucleus interactions. The binding potentials for the $N\Delta$ and NN^* channels were assumed to be 0.6 times that of the NN channel; the parameters are listed in Table II. The reduction in binding energy is based on the position of the quasifree Δ peak at low momentum transfer in (e,e') measurements[46] and should be regarded as only a crude estimate. Real and virtual Δ's were assumed to experience the same binding potential and no changes in the intrinsic widths of the Δ and N^* resonances were assumed to occur in the nuclear medium. Sensitivity to the Δ and N^* nuclear binding potentials was minimal (see Sec. III D).

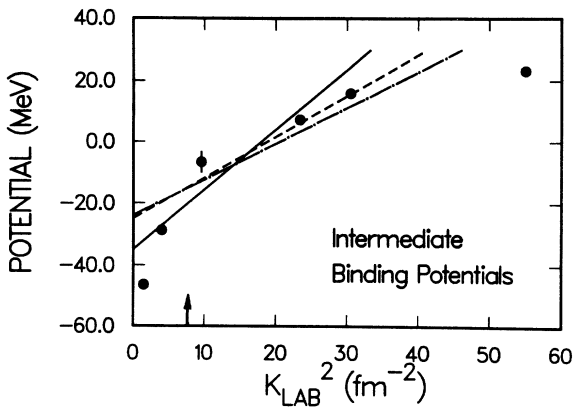

FIG. 5. Intermediate binding potentials assumed in the calculations compared with the real, central optical potential strengths at $r=0$ for $p+{}^{40}$Ca from Dirac phenomenology. The solid, dashed, and dashed-dotted lines indicate the primary NN channel potentials (see Table II) assumed for the 320, 400, and 650 MeV calculations, respectively. The results from Dirac phenomenology (closed circles) are from Ref. 45. The arrow indicates the value of $(K_{\text{lab}}/2)^2$ for 500 MeV protons.

D. Proton-nucleus elastic scattering

The nonrelativistic microscopic optical model of Refs. 4 and 35 for proton-nucleus elastic scattering was evalu-

TABLE II. Intermediate binding potential parameters for $k_F=1.4$ fm^{-1}.

Energy (MeV)	Channel (α)	$A_{\alpha,1}$ (MeV)	$A_{\alpha,2}$ (MeV)	B_α (MeV fm^2)
		Primary values		
320	NN	-50	-35	1.95
	N-isobar	-30	-21	1.17
400,500	NN	-50	-25	1.33
	N-isobar	-30	-15	0.75
650,800	NN	-50	-24	1.17
	N-isobar	-30	-14.4	0.70
		Alternate values		
320	NN	-50	-40	3.06
	N-isobar	-30	-24	1.84
400,500	NN	-50	-30	2.25
	N-isobar	-30	-18	1.35
650,800	NN	-50	-18	0.75
	N-isobar	-30	-10.8	0.45

ated where two-body target nucleon correlation contributions were included and the scattering observables were determined by solving the Schrödinger equation with relativistic kinematics.[4] A brief description of this part of the calculation follows.

The first-order optical potential was calculated assuming the local density approximation according to the following (in the notation of Ref. 4):

$$U_{\rm opt}^{(1)}(r)=(2\pi)^{-3}\sum_{j=p,n}\left[\int_0^\infty 4\pi q^2 dq\, t_{pj}^{a}(q,\rho(r))\tilde{\rho}_j(q)j_0(qr)+\frac{i}{r}\frac{\partial}{\partial r}\int_0^\infty 4\pi q^2 dq\, \tilde{t}_{pj}^{c}(q,\rho(r))\tilde{\rho}_j(q)j_0(qr)\sigma\cdot l\right], \quad (13)$$

where

$$\tilde{t}_{pj}^{c}(q,\rho(r))=\frac{t_{pj}^{c_0}(q,\rho(r))}{(K_{\rm on})^2\sin\theta_N}, \quad (14)$$

subscript j refers to target neutrons or protons, $K_{\rm on}$ is the pA COM on-shell momentum, and θ_N is defined by $q=2K_{\rm on}\sin(\theta_N/2)$ where q is the momentum transfer. The NN density dependent t matrices [from Eq. (12)] were evaluated at the finite nuclear density ρ at the position of the projectile.[47,48] Sensitivity to the coordinate position at which the effective interaction was evaluated is small at intermediate energies according to Ref. 47.

The proton densities for ^{16}O, ^{40,48}Ca, and ^{208}Pb were obtained by unfolding the single proton electric form factor from the measured nuclear charge densities[49–52] including separate corrections for the neutron electric and nucleon magnetic form factors.[35,53] For the absolute predictions the neutron densities were determined by adding the neutron-proton density difference from the Hartree-Fock-Bogoliubov (HFB) distributions of Dechargé and Gogny[54] to the empirical proton density as in Eq. (29) of Ref. 4. For the calculations in which the differential cross section data were fitted, the neutron densities also included a difference of two Woods-Saxon forms as in Eq. (30) of Ref. 4. This model contains two pairs of surface geometry parameters; one set was varied to fit the data while the other, a reference set, was held fixed. The latter quantities are given in Ref. 4.

Second-order optical potential contributions due to Pauli, short-range dynamical, and center-of-mass correlations in the target wave function were added.[35] Gaussian parametrizations of the low q components of the free NN Breit frame t matrices were used along with the correlation lengths given in Ref. 35.

III. RESULTS

Density dependent calculations were carried out for laboratory proton kinetic energies of 300, 320, 400, 500, 613, 650, and 800 MeV for ^{16}O, ^{40}Ca, ^{48}Ca, and ^{208}Pb. The medium modifications to the isoscalar, spin-independent, and spin-orbit amplitudes and to the predicted proton-nucleus elastic scattering observables are discussed in this section. The effects on deduced nuclear structure information, sensitivity to the binding energy parameter values, and requirements of self-consistency are also discussed in the following.

A. Density dependence of effective NN t matrix

Medium modifications to t_0 and t_0^{LS} at 500, 650, and 800 MeV are shown in Figs. 6–9 where the solid, dotted, and dashed lines correspond to $k_F=1.4$, 0.7, and 0.0 fm^{-1}, respectively. The t matrices were evaluated in the NN COM frame by multiplying the amplitudes in Eq. (11) by $-4\pi(\hbar c)^2/\varepsilon_{NN,\rm c.m.}$ where $\varepsilon_{NN,\rm c.m.}$ is the total on-shell relativistic energy of each nucleon in the NN COM frame. The t matrices represented in Figs. 6–9 were computed directly from the model and do not correspond to the scaled quantities in Eq. (12).

From the results in Figs. 6–9 the following effects due to medium modifications are observed: (1) Re(t_0) is increased overall yielding a less attractive real, central optical potential; (2) Im(t_0) is suppressed at low momentum

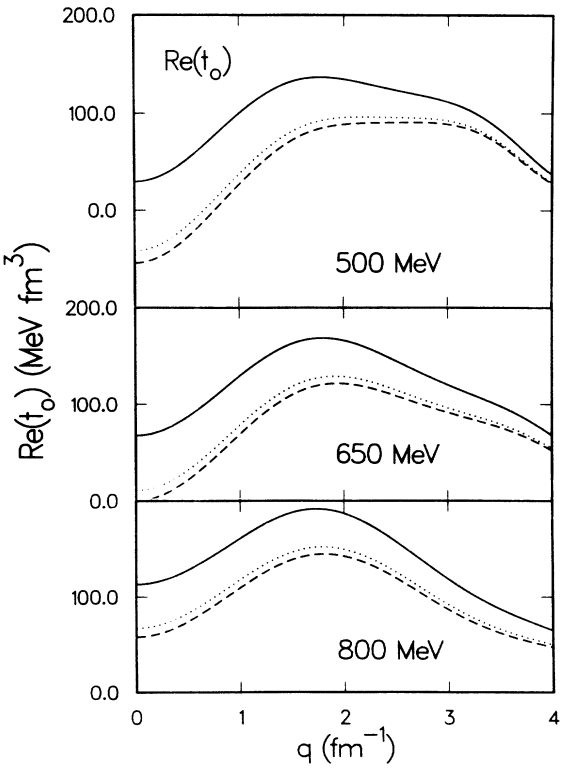

FIG. 6. Model calculations of the density dependence for Re(t_0) at 500, 650, and 800 MeV in the NN COM. The solid, dotted, and dashed lines correspond to $k_F=1.4$, 0.7, and 0.0 fm^{-1}, respectively.

transfer but is slightly enhanced for q greater than 3 fm^{-1}; (3) Re(t_0^{LS}) (which determines the imaginary part of the pA spin-orbit potential) is enhanced at low q; (4) Im(t_0^{LS}) (which determines the real spin-orbit potential) is enhanced overall; (5) the size of the effects decreases rather slowly with increasing incident beam energy; and (6) the corrections depend nonlinearly on k_F. The density dependences of Re(t_0), Im(t_0), and Im(t_0^{LS}) are qualitatively similar to that obtained at 135 MeV (see Ref. 47) by the Hamburg group[7–9] using both the Hamada-Johnston and Paris NN interactions and by Nakayama and Love[10] using the Bonn potential. The density dependence of the small Re(t_0^{LS}) amplitude tends in the opposite direction from the calculations at 135 MeV using the aforementioned NN interactions. The continued importance of medium corrections at 800 MeV is somewhat unexpected.

B. Elastic scattering observables

In Figs. 10–18 calculations with and without medium corrections are compared with each other and with data[2,3,36,55–65] for complete sets of elastic scattering observables. The references for the data are summarized in Table III. Differential cross sections are shown in Figs. 10–12, analyzing powers (A_y) are displayed in Figs. 13–15, and spin rotation parameters (Q) are given in Figs. 16–18. Predictions with and without medium corrections are indicated by the solid and dashed curves, respectively.

At ~300, 400, and 500 MeV the differential cross section predictions including medium modifications do not display diffractive minima which are as deep as that predicted by calculations based on the impulse approximation and are in overall better agreement with the data. The general shapes of the experimental angular distributions are reproduced fairly well by the predictions which include medium modifications. One exception is $p+^{208}$Pb at 500 MeV for which insufficient improvement is predicted. Also the predicted minima occur at somewhat smaller angles than that of the data indicating that the overall size of the optical potentials is too large. At ~650 and 800 MeV the medium corrections to the differential cross section predictions are not very great although at large angles the calculations with density dependence are shifted outward in angle and lowered in magnitude, which improves agreement with the 800 MeV large angle cross section data.[64] The predicted optical potentials at these higher energies are also too large. The medium modifications to the 300 MeV $p+^{40}$Ca and 400 MeV $p+^{208}$Pb differential cross section predictions agree with similar calculations based on the Paris-Hamburg density dependent interaction.[66]

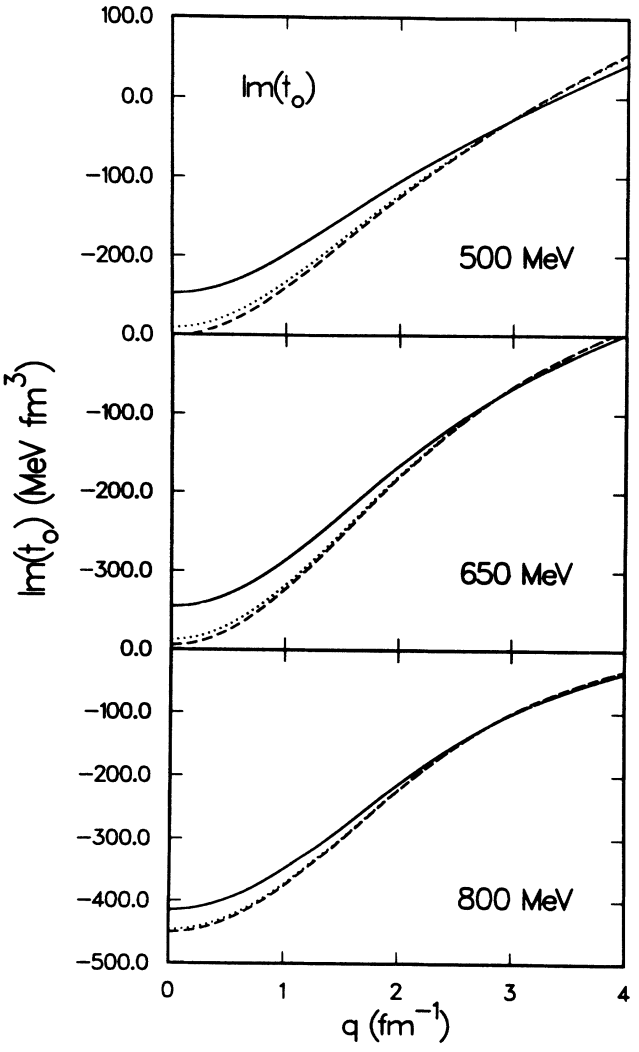

FIG. 7. Same as Fig. 6, except Im(t_0).

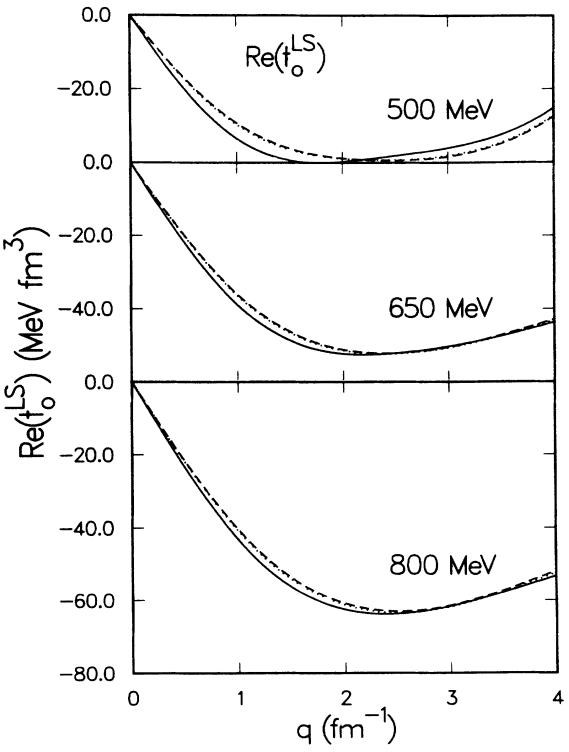

FIG. 8. Same as Fig. 6, except Re(t_0^{LS}).

TABLE III. Reference numbers for proton-nucleus elastic scattering data.

T_L	^{16}O			^{40}Ca			^{208}Pb		
(MeV)	$\frac{d\sigma}{d\Omega}$	A_y	Q,β	$\frac{d\sigma}{d\Omega}$	A_y	Q,β	$\frac{d\sigma}{d\Omega}$	A_y	Q
300				59	59		59	59	61
320	55,56	55,56			55,56	55			
400				59	59	55	59	59	
500	55,56	55,56	55,56	2	2	3	2	2	62
613				60					
650	55	55	55		55	55	63	63	
800	57	57	58	36	36	58	64	65	58

Recently it was shown that the 500 MeV forward angle differential cross section predictions in the Coulomb-nuclear interference (CNI) region are very sensitive to relativistic dynamics.[67] Enhancements in this region of from 10–20% relative to the NR value are predicted for 500 MeV $p+^{40}$Ca and ^{208}Pb using the relativistic impulse approximation (RIA)–Dirac equation model.[4] Medium effects in the CNI angular region for these two cases produce enhancements relative to the NRIA prediction of only about 5%. The RIA differential cross section predictions at forward angles are also 10–20% larger than the NR density dependent predictions.

Density dependence significantly affects the $p+^{16}$O A_y predictions (Fig. 13) resulting in an overall improvement between theory and experiment. Discrepancies remain at forward angles where relativistic dynamics produce dramatic effects.[21–23]

The $p+^{40}$Ca analyzing power predictions and data are shown in Fig. 14. At 300, 400, and 500 MeV quantitative

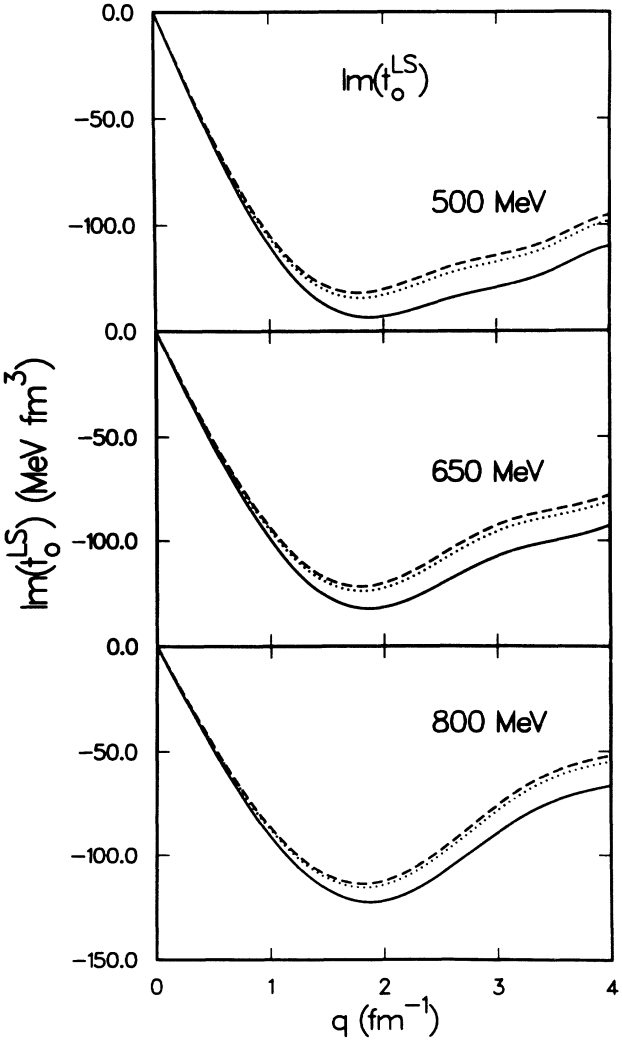

FIG. 9. Same as Fig. 6, except Im(t_0^{LS}).

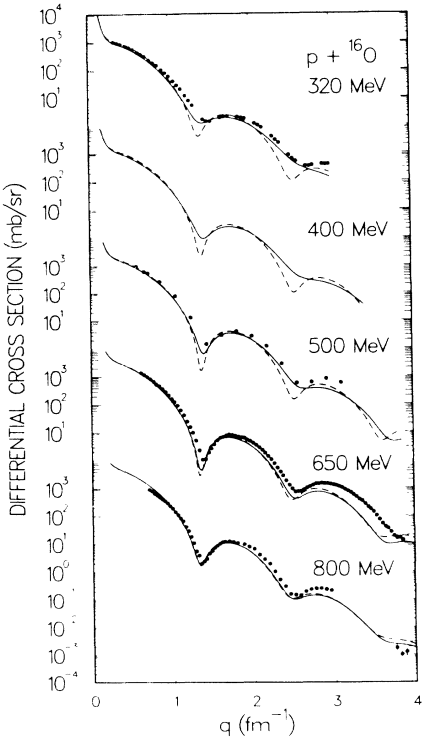

FIG. 10. Differential cross section predictions and data for $p+^{16}$O elastic scattering at various energies. The solid and dashed curves indicate the NR predictions based on the present density dependent model or on the IA, respectively, as discussed in the text. Refer to Table III for references to the data.

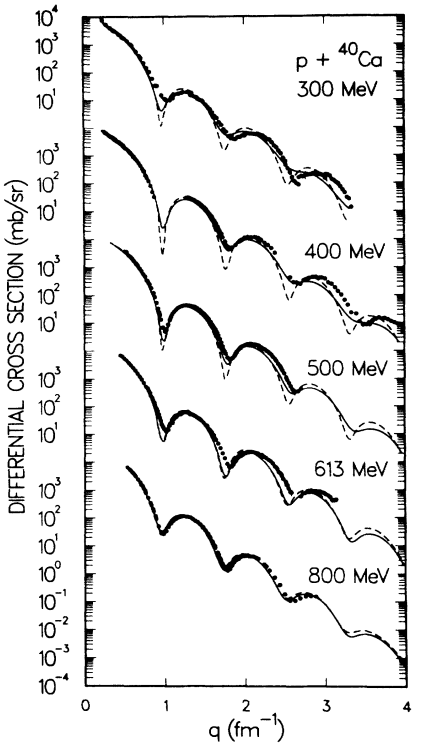

FIG. 11. Same as Fig. 10, except differential cross sections for $p + {}^{40}\mathrm{Ca}$.

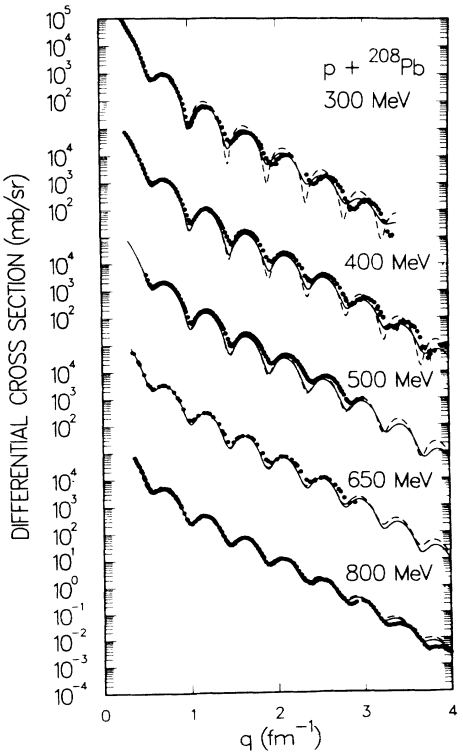

FIG. 12. Same as Fig. 10, except differential cross sections for $p + {}^{208}\mathrm{Pb}$.

descriptions of the data are obtained with the density dependent model except at forward angles. Improved descriptions also result at 650 and 800 MeV although the effects due to medium modifications are smaller than at 500 MeV and below.

The $p + {}^{208}\mathrm{Pb}$ analyzing power results in Fig. 15 are

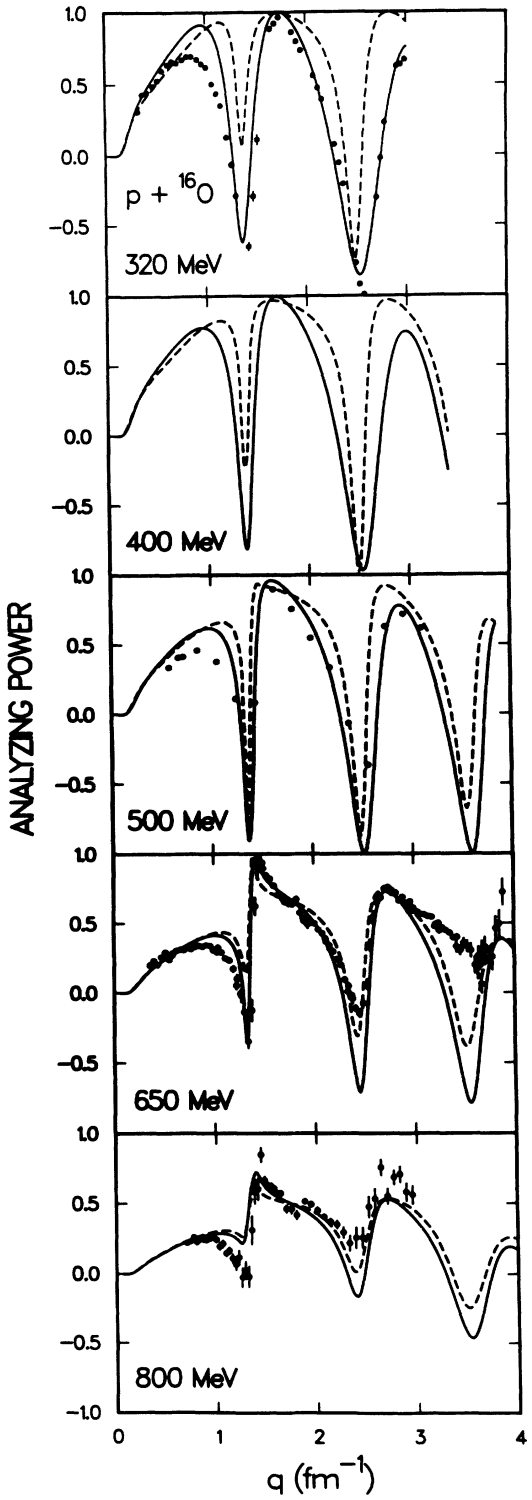

FIG. 13. Same as Fig. 10, except analyzing powers for $p + {}^{16}\mathrm{O}$.

similar to that for ^{40}Ca. Considerable improvement in the description of the 300, 400, and 500 MeV data results at all but the more forward angles where discrepancies with the data remain. Medium corrections are not as important at 650 and 800 MeV. The density dependent effects shown here for $p+^{40}$Ca A_y at 300 MeV and $p+^{208}$Pb A_y at 400 MeV are very similar to that computed using the Paris-Hamburg density dependent interaction.[66]

Spin rotation predictions and data for $p+^{16}$O are

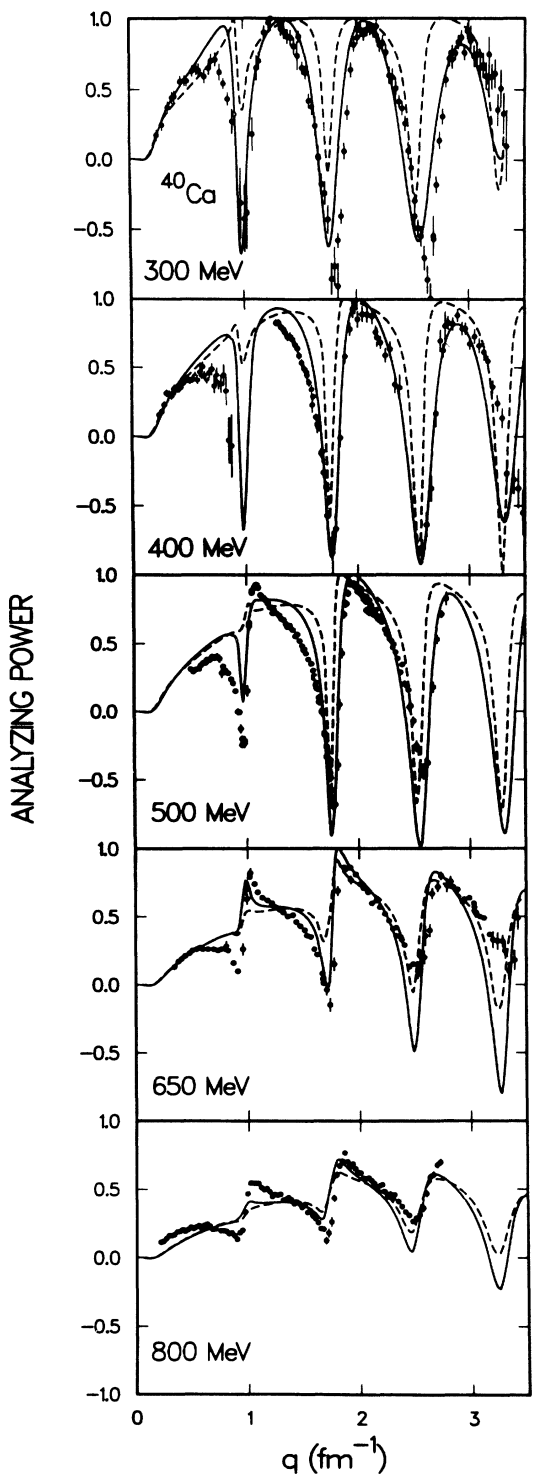

FIG. 14. Same as Fig. 10, except analyzing powers for $p+^{40}$Ca.

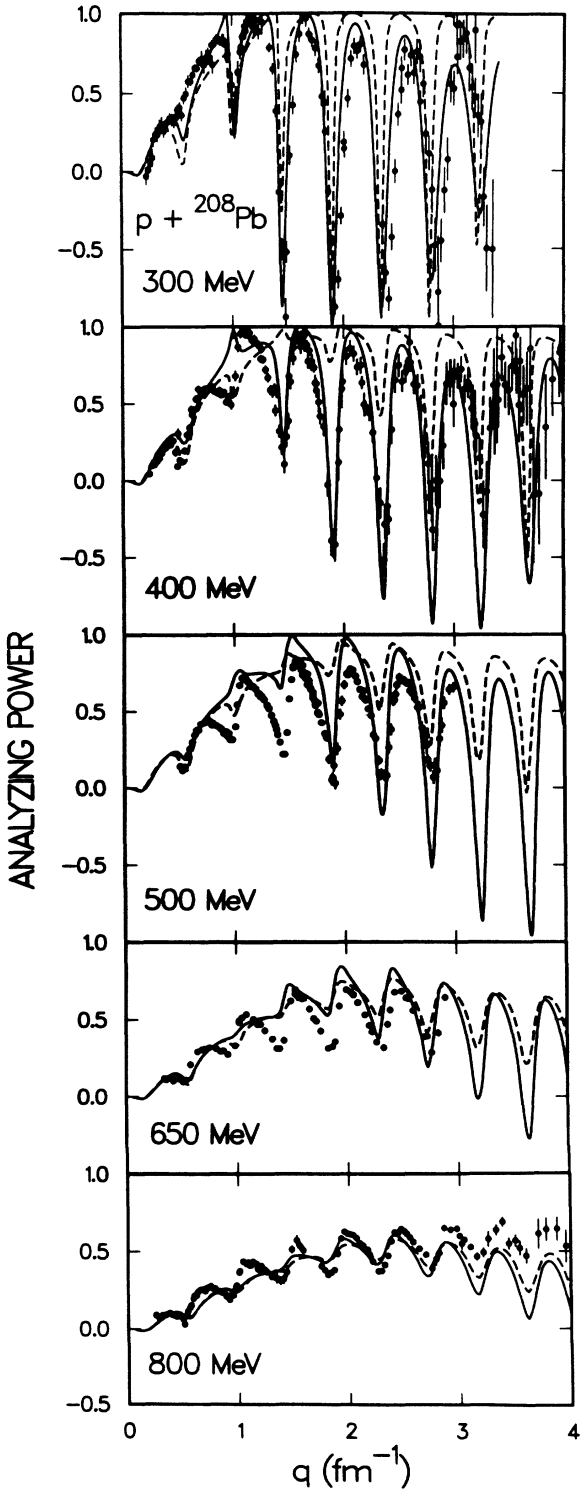

FIG. 15. Same as Fig. 10, except analyzing powers for $p+^{208}$Pb.

shown in Fig. 16. At 650 MeV the spin rotation data are presented in terms of the rotation angle β where[68]

$$\sin\beta = \frac{Q}{(1-P^2)^{1/2}} \ . \tag{15}$$

Dramatic improvement in the theoretical description of the 500 MeV Q data results when medium corrections are included. The effects of density dependence gradually become less important as the laboratory energy is increased.

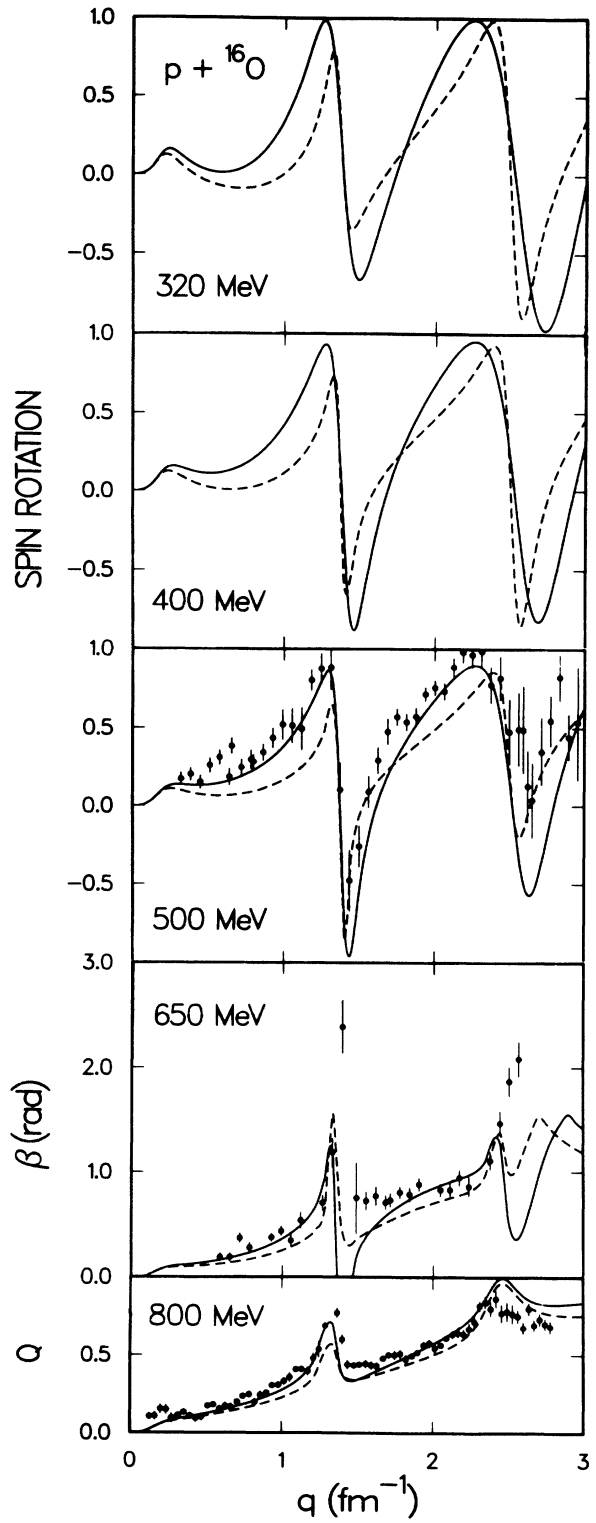

FIG. 16. Same as Fig. 10, except spin rotation parameters for $p + {}^{16}\mathrm{O}$.

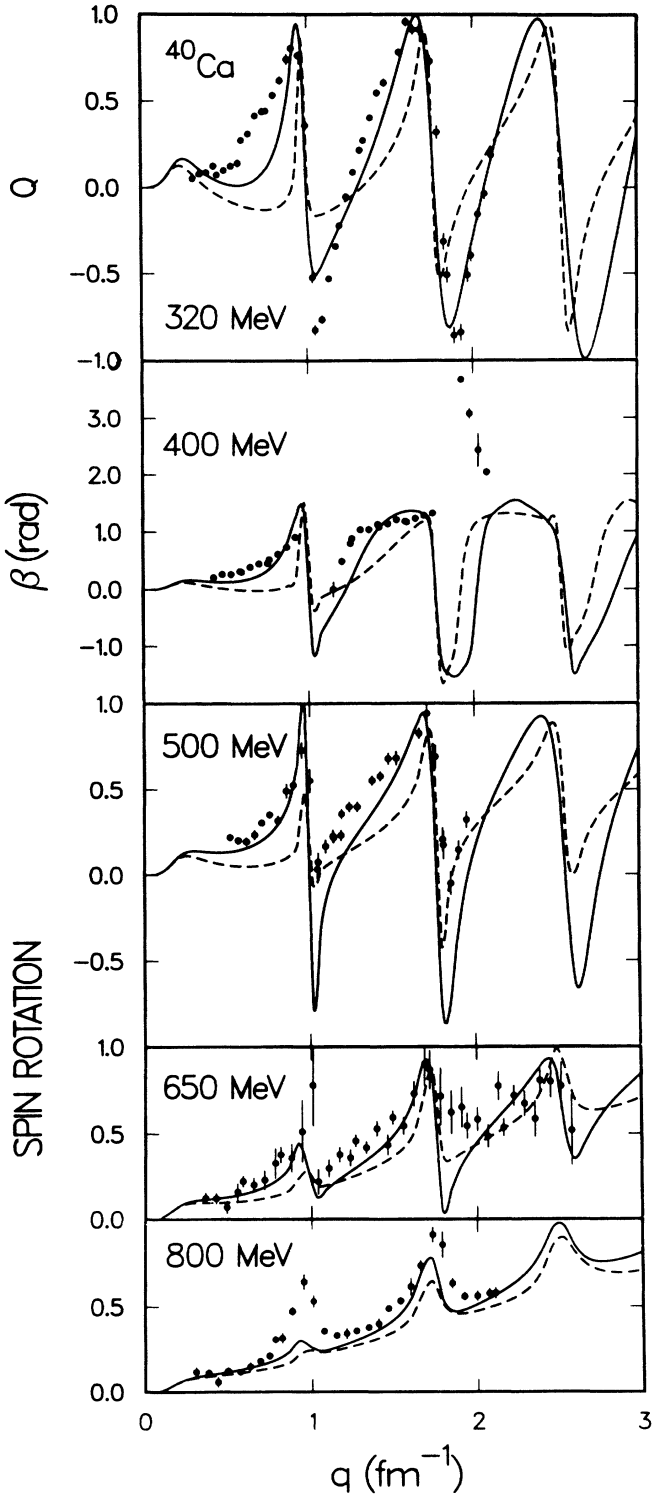

FIG. 17. Same as Fig. 10, except spin rotation parameters for $p + {}^{40}\mathrm{Ca}$.

Overall the nonrelativistic model with medium corrections reproduces the available $p+{}^{16}O$ Q data fairly well.

The spin rotation predictions and data for $p+{}^{40}Ca$ are displayed in Fig. 17. At 400 MeV the spin rotation angle β is shown. Overall, calculations including medium corrections produce significantly better fits to the data for each case. Calculations of off-shell and full-folding effects at 300 MeV (Ref. 14) suggest that further improvement in the NR description of the 320 MeV $p+{}^{40}Ca$ Q data might result if these and medium effects were combined in the calculations. The fit to the 500 MeV Q data is much improved but is not as impressive as that obtained with the RIA–Dirac equation model.[19,20]

Spin rotation predictions and data for $p+{}^{208}Pb$ are shown in Fig. 18. Medium corrections again improve the agreement between NR theory and data; however, significant discrepancies remain at each energy, particularly at forward angles. Off-shell and full-folding corrections might improve the quality of the theoretical predictions at 290 and 500 MeV; however, fairly large adjustments are required at 290 MeV to bring the predictions into agreement with the data. It is important to note that relativistic scattering model predictions[4,21,58] for these three sets of Q data are much more successful than the NR results shown here.

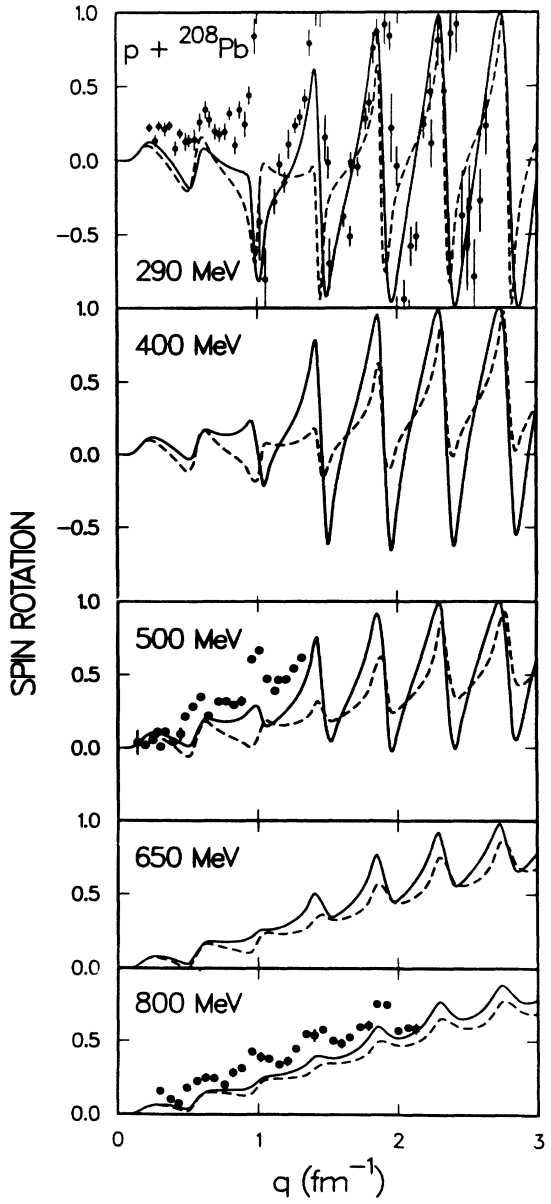

FIG. 18. Same as Fig. 10, except spin rotation parameters for $p+{}^{208}Pb$.

At 650 and 800 MeV the electromagnetic spin-orbit (EMSO) potential induces significant changes in the forward angle spin observables.[58,65,69] This electromagnetic interaction results from the relative motion between the projectile magnetic moment and the electrically charged nucleus. In Ref. 69 it is shown that the EMSO potential, when included in the nonrelativistic density dependent model described here, results in fairly good descriptions of the 650 and 800 MeV analyzing power and spin rotation data for targets ^{16}O, ^{40}Ca, and ^{208}Pb. The EMSO effects are quite large at these energies at forward angles (particularly for ^{40}Ca and ^{208}Pb); however, the medium corrections discussed here are instrumental in achieving the good overall description of the data in Ref. 69. EMSO effects are less important at lower energies.

It is interesting to separately display the Pauli blocking and intermediate binding energy contributions to the scattering observables. In Figs. 19 and 20 three sets of predictions are shown for $p+{}^{40}Ca$ at $\sim$300 and 500 MeV, respectively. The solid, dotted, and dashed lines in these figures represent calculations including both Pauli blocking and binding energy corrections, Pauli blocking only, and no medium modifications, respectively. At $\sim$300 MeV the induced changes in the observables due to Pauli blocking and binding energy corrections are similar in both magnitude and direction. At 500 MeV the effects due to binding energy are larger than those due to Pauli blocking (Fig. 20). At 800 MeV (not shown) almost all of the density dependent effects are due to the binding energy correction. Therefore the Pauli blocking contributions quickly diminish at higher energies as expected whereas significant binding energy effects persist even to 800 MeV.

C. Effects of density dependence on deduced neutron densities

In recent years attention has been given to the problem of deducing ground state neutron density distributions from NRIA analyses of the high quality 800 MeV pA elastic scattering data from the Los Alamos Meson Physics Facility (LAMPF).[34–36] It is therefore worthwhile to evaluate the impact which nuclear medium corrections have on deduced nuclear structure information. Both absolute and relative neutron distributions were studied in this work.

A sensitive test of microscopic models of pA elastic scattering is to compare the deduced neutron distributions with the "known" values for self-conjugate nuclei such as ^{40}Ca. The deduced neutron density should agree with the measured proton distribution and should not be dependent on the energy of the scattering measurement.

In order to obtain these quantities the model neutron densities were varied such that the overall diffractive structure of the predicted and experimental differential cross sections agreed as well as possible based on $|\chi|^2$ minimization.

In Fig. 21 root-mean-square (rms) radii are shown for the deduced neutron densities in ^{40}Ca obtained by fitting the available differential cross section data. The quantity Δr_{np} in the figure is defined by

$$\Delta r_{np} \equiv \langle r_n^2 \rangle^{1/2} - \langle r_p^2 \rangle^{1/2} ,$$

where $\langle r_j^2 \rangle^{1/2}$ are the rms radii for the j=proton (p) and neutron (n) distributions. For ^{40}Ca $\langle r_p^2 \rangle^{1/2}$ is 3.389 fm. The dashed line in the figure represents the theoretical value of -0.05 fm which is predicted by several models.[54,70] The deduced values of Δr_{np} based on calculations with and without medium modifications are indicat-

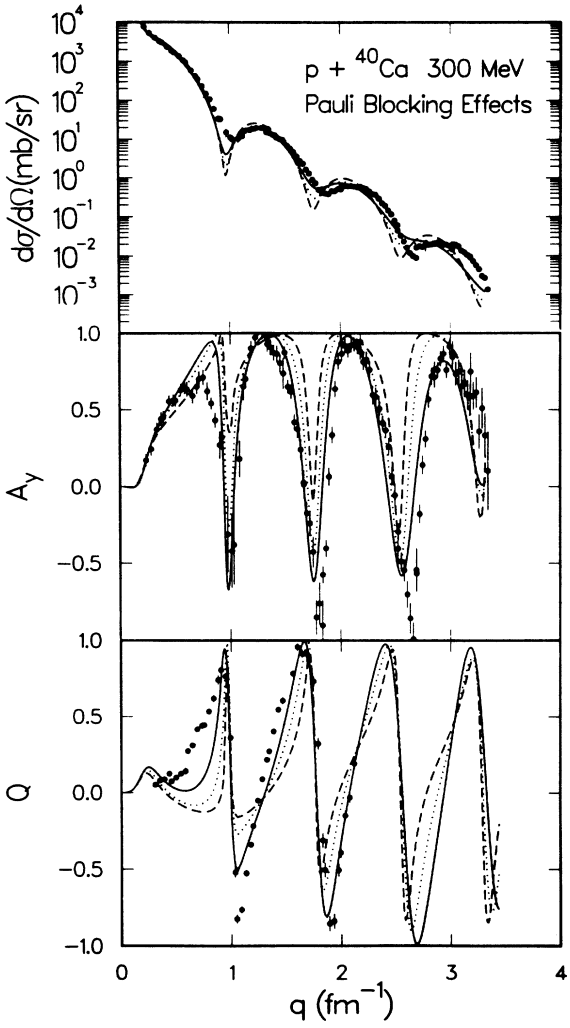

FIG. 19. Density dependent model predictions for 300 MeV $p+^{40}$Ca elastic scattering observables. The dashed, dotted, and solid curves represent calculations with no medium corrections, with Pauli blocking corrections only, and with both Pauli blocking and binding energy corrections, respectively, as discussed in the text. The data and calculations for Q are at 320 MeV.

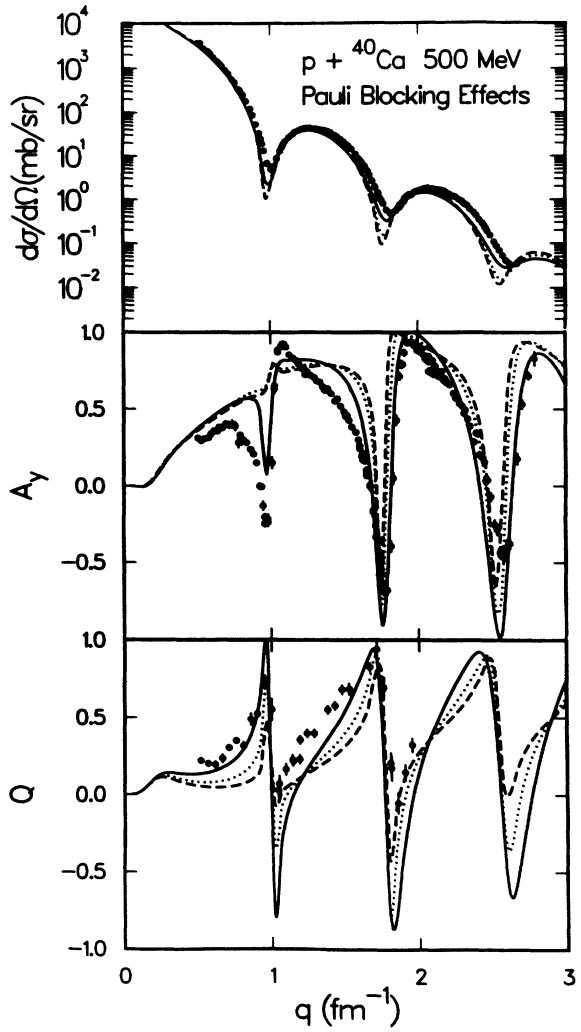

FIG. 20. Same as Fig. 19, except $p+^{40}$Ca at 500 MeV.

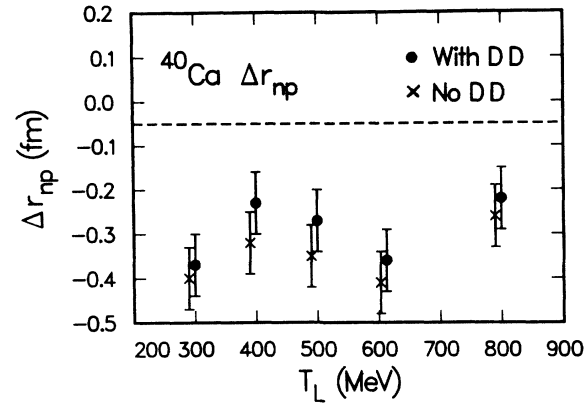

FIG. 21. Neutron-proton density rms radii differences for ^{40}Ca deduced using the NR density dependent model (closed circles) and the NRIA (crosses). The uncertainties of ± 0.07 fm reflect statistical and systematic error in the data, uncertainties in the free NN amplitudes, and uncertainties in the input to the fitting procedure (see Refs. 34 and 35). The theoretical value of -0.05 fm is indicated by the dashed line. The NRIA values are offset for visual clarity.

ed by the solid dots and crosses, respectively. Uncertainties of ±0.07 fm were assumed based on previous error analyses.[34,35] The inclusion of medium corrections in the analysis results in deduced values of Δr_{np} which are generally a little closer to the expected value; however, they remain about 0.2–0.3 fm too small. Similar $|\chi|^2$ analyses using relativistic models[4] obtain larger Δr_{np} values for $T_{\rm lab} \geq 500$ MeV but they are not energy independent and are not in agreement with expectations for self-conjugate nuclei.

It has been argued that microscopic analyses of 800 MeV proton-nucleus elastic scattering data from neighboring isotopes result in reliable values for the relative isotopic neutron density differences.[35,36] The 800 MeV $p+{}^{40}$Ca and ^{48}Ca differential cross section data were analyzed using $|\chi|^2$ minimization with the present NR model both including and not including medium corrections. The ^{48}Ca-^{40}Ca neutron rms radii differences were determined to be 0.19±0.05 fm in both cases. This agrees very well with the HFB prediction of 0.20 fm.[54] The differences between the ^{48}Ca and ^{40}Ca neutron distributions obtained from analyses with (solid line) and without (dashed line) medium corrections are shown in Fig. 22. The differences between the two curves are noticeable but are less than the uncertainty envelope for this case.[36] Therefore the neutron isotopic density differences deduced from microscopic NRIA analyses of 800 MeV proton-nucleus elastic scattering data are not significantly altered when medium corrections of the type considered here are included.

D. Sensitivity to binding energies, self-consistency requirement

The adequacy of the simple quadratic form ($U = A + B\kappa^2$) of the intermediate binding potential was tested by studying the sensitivity of the calculated results to variations in the parameters A and B using the alternate binding potential parameters in Table II. The alternate parameter sets were chosen such that the binding potentials agreed with those of the primary set and with

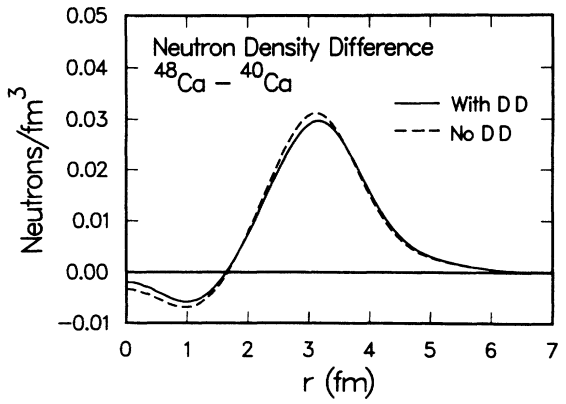

FIG. 22. Comparison of the ^{48}Ca-^{40}Ca neutron density differences deduced at 800 MeV using the NR density dependent model (solid curve) and the NRIA (dashed curve) as explained in the text.

Dirac phenomenology[45] at $K_{\rm lab}/2$ but differed at lower and higher values of momentum. For the 300 and 500 MeV cases the alternate potentials agreed better with Dirac phenomenology at lower momentum whereas for the 800 MeV case the alternate potential agreed better with phenomenology at higher momentum. Results of calculations with density dependence for $p+{}^{40}$Ca at 300, 500, and 800 MeV using both the primary and alternate binding potentials were compared. The differences between the predicted observables were negligible, hence the density dependent predictions are insensitive to large changes in the assumed intermediate binding potentials at momentum values much larger or smaller than $K_{\rm lab}/2$. Since the binding energy correction is mainly dependent on a relatively confined region of momentum, the simple $A + B\kappa^2$ form for $U(\kappa^2)$ is adequate.

The sensitivity to the Δ-nucleus binding potential was also studied where the $N\Delta$ channel parameters in Table II were replaced by the primary NN values. The results for 500 MeV $p+{}^{40}$Ca are shown in Fig. 23. The density dependent predictions based on the primary NN and $N\Delta$-channel parameters are indicated by the solid lines while the dotted lines display the alternate results. The effects are noticeable but not very large. Less sensitivity was found at 800 MeV in similar calculations. The predictions were completely insensitive to analogous changes in the binding potentials for the NN^* channels. It is fortunate that the predicted pA elastic scattering observables were not very sensitive to the poorly known isobar-nucleus interaction potentials.

The sensitivities of the density dependent NN amplitudes to the following changes in various elements of the model were also studied: (1) arbitrary 10% increases in the intrinsic isobar widths, (2) including or not including Pauli blocking of the Δ and N^*, (3) use of relativistic or nonrelativistic kinematics for the angle averaged Pauli blocking factor, and (4) arbitrary 5 MeV changes in the struck nucleon binding energy parameter $A_{\alpha,1}$ (see Appendix B). Each of these variations in the calculations resulted in small changes in the density dependent amplitudes for $k_F = 1.4$ fm^{-1}. The lack of sensitivity to Δ-blocking supports the Paris-Hamburg effective interaction model[8,9] which does not treat virtual Δ propagation explicitly.

For the unsymmetrized Watson t matrix there is no formal requirement that the assumed intermediate nucleon binding potential $U(\kappa^2)$ be consistent with that calculated in Eq. (13) for the (distinct) projectile. In practice, of course, for nucleon-nucleus scattering self-consistency between the input and calculated real, central potentials should be obtained. The interior strengths of the real, central $p+{}^{40}$Ca optical potentials computed at 300, 500, and 800 MeV were therefore compared with the analogous quantities from Dirac phenomenology[45] (see Fig. 5). Over the relevant range of momentum the calculated potentials were about 5 MeV more attractive than the empirical values which themselves are uncertain by at least this amount.[71] The input binding potentials were accordingly made 5 MeV more attractive and new density dependent calculations were run for 500 MeV $p+{}^{40}$Ca. The subsequent change in the computed real,

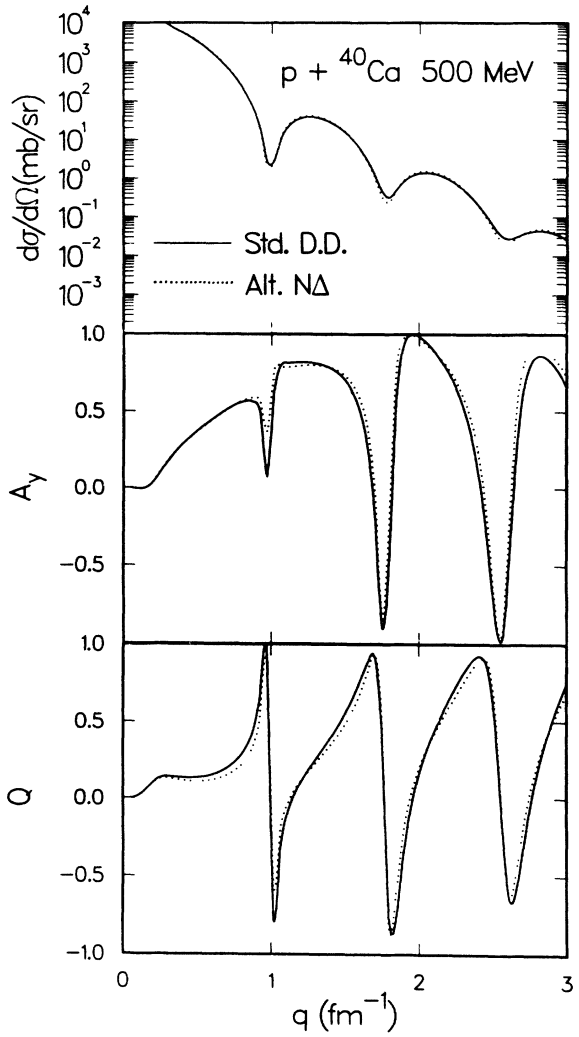

FIG. 23. Effects of alternate Δ-nucleus binding potential for 500 MeV $p+{}^{40}$Ca elastic scattering. The solid curves represent calculations based on the primary $N\Delta$ channel binding energy parameters given in Table II and are identical to the solid curves in Figs. 11, 14, and 17 for 500 MeV. The dotted curves show the results of a calculation in which the $N\Delta$ channel binding energy was set equal to that of the NN channel. See text for further discussion.

central well depth was only 0.6 MeV and the changes in the scattering observables were completely negligible. The calculations very quickly achieved self-consistency in only one iteration; very minute changes occurred in the predicted scattering observables. Therefore, the calculations presented here assuming the Dirac phenomenological input are, for practical purposes, self-consistent.

IV. CONCLUSIONS

Medium modifications to the nonrelativistic NN effective interaction are well known to be important at energies of a few hundred MeV. In this work it was shown that medium corrections are also significant at higher bombarding energies above 300 MeV, even up to 800 MeV. Pauli blocking effects were shown to quickly diminish with increased beam momentum as expected. Binding energy effects, on the other hand, remained significant at 500 MeV and continued to produce small but significant changes in the predicted observables at 800 MeV. Because of the importance of the off-shell dependence of the NN interaction in determining the binding energy corrections, these calculations should be repeated using other NN interaction models.[16,72,73]

The nonrelativistic, density dependent model predictions for proton-nucleus elastic scattering are much better than NRIA predictions for beam energies up to 650 MeV. At all energies studied the forward angle differential cross section data and the analyzing power and spin rotation data from $q \simeq 1-3$ fm^{-1} are now generally well described by the NR approach (if EMSO terms are also included at 650 and 800 MeV).[69] Further improvement in the NR model predictions might also result when NN t-matrix off-shell dependences and full-folding calculations are combined with medium corrections. A numerical evaluation of the full first-order Watson optical potential (for uniform nuclear matter using the LDA) is now possible to do and should be carried out in the future. If serious discrepancies between the full, first-order NR model predictions and data remain then it is likely that further dynamics, beyond that contained in NR multiple scattering theory, will be required to explain the data.

This work demonstrates that much of the success of the relativistic approach can also be achieved with NR models. Deficiencies remain in the NR predictions for the forward angle ($q \leq 1$ fm^{-1}) spin observables where recent relativistic scattering models display very good agreement with data.[4,19-24] Studies of relativistic processes in nucleon-nucleus scattering should probably focus on this low momentum transfer region below about 1.5 fm^{-1}. Calculations of the relativistic NN effective interactions are well advised to include binding energy corrections and off-shell dependences in the positive energy NN sector. Full-folding calculations of the relativistic optical potential should also be carried out.

With respect to nuclear structure studies using intermediate energy proton-nucleus scattering the problem of deducing the correct nuclear matter distribution for ^{40}Ca remains.[4] Analyses of $p+{}^{40}$Ca differential cross section data using NRIA or density dependent models obtain a deduced neutron density rms radius which is about 0.2–0.3 fm too small. On the other hand, isotopic neutron density differences obtained in NRIA analyses[35,36] of 800 MeV proton elastic scattering data appear to be reliable and accurate.

The explicit treatment of Δ intermediate scattering states in the proton-nucleus elastic scattering process turns out not to be very important. The calculations are not very sensitive to the assumed Δ-nucleus binding potential, to Δ blocking in intermediate states, or to the intrinsic properties of the Δ in the nuclear medium. This lack of sensitivity supports the Paris-Hamburg and similar effective interaction models at lower energies.[5-12] Of course Δ production is a straightforward and reasonable way to account for the large NN inelasticities in the $T=1$ partial wave channels and improved information con-

cerning the Δ-nucleus interaction and properties of the Δ in nuclear matter would be useful to incorporate in the model.

The present work makes it clear that new physics issues associated with relativistic dynamics, possible changes in the bound nucleon form factors, variation in meson masses in the nuclear medium, etc., can only be reasonably studied when the physics included in conventional NR multiple scattering theory has been fully exploited in the numerical applications. Furthermore, any new reaction dynamics or structure effects will only be allowed to make fairly small net changes in the predicted observables in order to maintain agreement with data.

Finally, the present model also predicts significant density dependence for some of the other spin and isospin components of the *NN* effective interaction which are not used in first-order models for elastic scattering from spin-zero nuclei. Application of this *NN* effective interaction to charge exchange and inelastic transitions at intermediate energies will be the subject of another article.

ACKNOWLEDGMENTS

The author thanks Professor H. V. von Geramb for helpful discussions related to the numerical solution of integral equations. This research was supported in part by the U.S. Department of Energy.

APPENDIX A

The expressions for the angle averaged *NN*, *NΔ*, and *NN** Pauli blocking operators using relativistic kinematics to relate the two-body COM and laboratory quantities are given here. The *NN* Pauli blocking operator is defined by requiring that

$$Q^{NN}(\mathbf{K}'_{NN,1},\mathbf{K}'_{NN,2},k_F)=1 \text{ if } |\mathbf{K}'_{NN,1}|>k_F \text{ and } |\mathbf{K}'_{NN,2}|>k_F$$
$$=0 \text{ otherwise }, \tag{A1}$$

where $\mathbf{K}'_{NN,1}$ and $\mathbf{K}'_{NN,2}$ are the intermediate momenta in the laboratory for nucleons 1 and 2 (see Appendix B) and k_F is the Fermi momentum of the nuclear medium. The total (conserved) momentum $\mathbf{P}$ is given by

$$\mathbf{P}=\mathbf{K}_{NN,1}+\mathbf{K}_{NN,2}=\mathbf{K}'_{NN,1}+\mathbf{K}'_{NN,2}\ , \tag{A2}$$

where $\mathbf{K}_{NN,1}$ and $\mathbf{K}_{NN,2}$ are the initial *NN* laboratory momenta. The momentum vectors $\mathbf{K}'_{NN,1}$ and $\mathbf{K}'_{NN,2}$ are given in terms of the *NN* COM intermediate wave number k'_{NN} and angle $\theta_{\text{c.m.}}$ (between $\mathbf{k}'_{NN}$ and $\mathbf{P}$) as

$$\mathbf{K}'_{NN,\{1,2\}}=\pm\hat{\mathbf{P}}_{\perp}k'_{NN}\sin\theta_{\text{c.m.}}+\hat{\mathbf{P}}_{\parallel}\left[\frac{P}{2}\pm\gamma k'_{NN}\cos\theta_{\text{c.m.}}\right]\ , \tag{A3}$$

where

$$\gamma=\left[1-\frac{P^2}{4k'^2_{NN}+4m_N^2+P^2}\right]^{-1/2}\ , \tag{A4}$$

the (plus) and (minus) signs apply for nucleons 1 and 2, respectively, $\hat{\mathbf{P}}_{\perp}$ and $\hat{\mathbf{P}}_{\parallel}$ are unit vectors perpendicular and parallel to $\mathbf{P}$ in the plane defined by $\mathbf{K}'_{NN,1}$ and $\mathbf{K}'_{NN,2}$, and m_N is the nucleon mass. The angle averaged *NN* Pauli blocking factor is obtained by computing the integral

$$Q^{NN}_{AV}(k'_{NN},P,k_F)=\frac{1}{4\pi}\int d\hat{\mathbf{k}}'_{NN}Q^{NN}(\mathbf{K}'_{NN,1},\mathbf{K}'_{NN,2},k_F)\ . \tag{A5}$$

Using Eqs. (A1)–(A5) the result is

$$Q^{NN}_{AV}=1 \text{ if } \left|\frac{P}{2}-\gamma k'_{NN}\right|>k_F$$
$$=0 \text{ if } [(P/2)^2+k'^2_{NN}]\le k_F^2$$
$$=\frac{\gamma P}{2(\gamma^2-1)k'_{NN}}\left[1-\left[1-\frac{4(\gamma^2-1)(k'^2_{NN}+P^2/4-k_F^2)}{\gamma^2P^2}\right]^{1/2}\right], \text{ otherwise }. \tag{A6}$$

The usual result[5] is easily recovered in the NR limit. Since Fermi motion effects were ignored in this work P was fixed equal to the incident proton laboratory momentum K_{lab}. In the above and remaining equations $c=1$ is assumed.

For the nucleon-isobar channels the Pauli exclusion principle was assumed to apply only to the nucleon. For example, in the *NΔ* channel the Pauli blocking operator is defined such that

$$Q^{N\Delta}(\mathbf{K}'_{\alpha,N},\mathbf{K}'_{\alpha,\Delta},k_F)=1 \text{ if } |\mathbf{K}'_{\alpha,N}|>k_F$$
$$=0 \text{ if } |\mathbf{K}'_{\alpha,N}|\le k_F \tag{A7}$$

without regard to the value of $\mathbf{K}'_{\alpha,\Delta}$, where $\mathbf{K}'_{\alpha,N}$ and $\mathbf{K}'_{\alpha,\Delta}$ refer to the nucleon and Δ intermediate momenta, respectively, in the laboratory and for this case α is the $N\Delta$ channel. Using a method analogous to the preceding NN case the angle averaged Pauli blocking factor for the $N\Delta$ channel is given by

$$Q_{AV}^{N\Delta}=1 \text{ if } |(\gamma^2-1)^{1/2}\varepsilon_N-\gamma k'_{N\Delta}|>k_F$$
$$=0 \text{ if } |(\gamma^2-1)^{1/2}\varepsilon_N+\gamma k'_{N\Delta}|\le k_F$$
$$=\frac{1}{2}\left\{1+\frac{\gamma\varepsilon_N}{(\gamma^2-1)^{1/2}k'_{N\Delta}}\left[1-\left[1-\frac{k'^2_{N\Delta}+(\gamma^2-1)\varepsilon_N^2-k_F^2}{\gamma^2\varepsilon_N^2}\right]^{1/2}\right]\right\} \text{ otherwise }, \tag{A8}$$

where for the $N\Delta$ case

$$\gamma=\left[1-\left[\frac{P}{E_N+E_\Delta}\right]^2\right]^{-1/2}, \tag{A9a}$$

$$(E_N+E_\Delta)^2=(\varepsilon_N+\varepsilon_\Delta)^2+P^2, \tag{A9b}$$

and

$$\varepsilon_{N,\Delta}=(k'^2_{N\Delta}+m^2_{N,\Delta})^{1/2}. \tag{A9c}$$

In Eq. (A9c) m_Δ is the mass of the Δ. Similar relations are used for the NN^* channel.

APPENDIX B

The form of the energy denominator of the Green's function in the Watson NN t matrix assumed here is given by

$$e_\alpha=E^{(1)}(\mathbf{K}_{\alpha,1})+E^{(2)}(\mathbf{K}_{\alpha,2})-E^{(1)}(\mathbf{K}'_{\alpha,1})-E^{(2)}(\mathbf{K}'_{\alpha,2})+i\varepsilon, \tag{B1}$$

where α denotes NN, $N\Delta$, or NN^* channels, superscripts (1) and (2) refer to the two particles (nucleons or isobars), $\mathbf{K}_{\alpha,1}$ and $\mathbf{K}_{\alpha,2}$ are the initial momenta, and $\mathbf{K}'_{\alpha,1}$ and $\mathbf{K}'_{\alpha,2}$ are the intermediate momenta. The momentum values are measured with respect to the nuclear medium which corresponds to the laboratory reference frame. Explicitly e_α is given by

$$e_\alpha=\frac{\hbar^2}{2m_{1,\alpha}}K^2_{\alpha,1}+\left[\frac{\hbar^2}{2m_{2,\alpha}}K^2_{\alpha,2}+A_{\alpha,1}+B_\alpha K^2_{\alpha,2}\right]-\frac{\hbar^2}{2m_{1,\alpha}}K'^2_{\alpha,1}-\left[\frac{\hbar^2}{2m_{2,\alpha}}K'^2_{\alpha,2}+A_{\alpha,2}+B_\alpha K'^2_{\alpha,2}\right]+i\varepsilon, \tag{B2}$$

where $m_{1,\alpha}$ and $m_{2,\alpha}$ are the particle masses in channel α.

For the target particle the kinetic energy and velocity dependent interaction terms can be combined by introducing an effective mass $\overline{m}_{2,\alpha}$ defined by

$$\overline{m}_{2,\alpha}\equiv(m^{-1}_{2,\alpha}+2B_\alpha/\hbar^2)^{-1}. \tag{B3}$$

Introducing total momentum $\mathbf{P}$ and initial and intermediate two-body COM momenta $\mathbf{k}_\alpha$ and $\mathbf{k}'_\alpha$, respectively, the energy denominator is finally expressed as (assuming nonrelativistic kinematics)

$$e_\alpha=\frac{\hbar^2}{2\bar{\mu}_\alpha}(\bar{k}^2_\alpha-k'^2_\alpha)+i\varepsilon, \tag{B4}$$

where

$$\bar{k}^2_\alpha=k^2_\alpha+\frac{2\bar{\mu}_\alpha}{\hbar^2}(A_{\alpha,1}-A_{\alpha,2}) \tag{B5}$$

and

$$\bar{\mu}_\alpha=m_{1,\alpha}\overline{m}_{2,\alpha}/(m_{1,\alpha}+\overline{m}_{2,\alpha}). \tag{B6}$$

The correct relativistic kinematic value for the initial COM momentum was used and the energy dependent isobar width[27] Γ_α (for the $N\Delta$ and NN^* channels) was included where k^2_α in Eq. (B5) was replaced with the complex quantity,

$$k^2_{\alpha,\mathrm{Rel}}+\frac{i\bar{\mu}_\alpha}{\hbar^2}\Gamma_\alpha.$$

The relativistic COM momentum was obtained from

$$k^2_{\alpha,\mathrm{Rel}}=\frac{\bar{s}}{4}-\frac{m^2_{1,\alpha}+\overline{m}^2_{2,\alpha}}{2}+\frac{1}{4\bar{s}}(m^2_{1,\alpha}-\overline{m}^2_{2,\alpha})^2,$$

where

$$\bar{s}=(m_{1,NN}+\overline{m}_{2,NN})^2+2T_L\overline{m}_{2,NN},$$

$\alpha=NN$ denotes the NN channel, and T_L is the incident nucleon laboratory kinetic energy.

[1]A. K. Kerman, H. McManus, and R. M. Thaler, Ann. Phys. (N.Y.) **8**, 551 (1959).
[2]G. W. Hoffmann *et al.*, Phys. Rev. Lett. **47**, 1436 (1981).
[3]A. Rahbar *et al.*, Phys. Rev. Lett. **47**, 1811 (1981).
[4]L. Ray and G. W. Hoffmann, Phys. Rev. C **31**, 538 (1985).
[5]J.-P. Jeukenne, A. Lejeune, and C. Mahaux, Phys. Rev. C **10**, 1391 (1974).
[6]F. A. Brieva and J. R. Rook, Nucl. Phys. **A291**, 299 (1977); **A291**, 317 (1977); **A297**, 206 (1978); **A307**, 493 (1978).
[7]H. V. von Geramb, F. A. Brieva, and J. R. Rook, in *Microscopic Optical Potentials*, edited by H. V. von Geramb (Springer-Verlag, Berlin, 1979), p. 104.
[8]H. V. von Geramb, in *The Interaction Between Medium Energy Nucleons in Nuclei (Indiana University Cyclotron Facility, Bloomington, Indiana, 1982)*, Proceedings of the Workshop on the Interactions Between Medium Energy Nucleons in Nuclei, AIP Conf. Proc. No. 97, edited by H. O. Meyer (AIP, New York, 1983), p. 44.
[9]L. Rikus, K. Nakano, and H. V. von Geramb, Nucl. Phys. **A414**, 413 (1984).
[10]K. Nakayama and W. G. Love, Phys. Rev. C **38**, 51 (1988).
[11]W. Haider, J. R. Rook, and A. M. Kobos, Nucl. Phys. **A480**, 20 (1988).
[12]N. Yamaguchi, S. Nagata, and J. Michiyama, Prog. Theor. Phys. (Jpn.) **76**, 1289 (1986).
[13]T. Cheon, Phys. Rev. C **35**, 2225 (1987).
[14]H. F. Arellano, F. A. Brieva, and W. G. Love, Phys. Rev. Lett. **63**, 605 (1989); University of Georgia report, 1989.
[15]Ch. Elster and P. C. Tandy, Phys. Rev. C **40**, 881 (1989); Ch. Elster, T. Cheon, E. F. Redish, and P. C. Tandy, *ibid.* **41**, 814 (1990).
[16]Ch. Elster, W. Ferchländer, K. Holinde, D. Schütte, and R. Machleidt, Phys. Rev. C **37**, 1647 (1988); Ch. Elster, K. Holinde, D. Schütte, and R. Machleidt, *ibid.* **38**, 1828 (1988).
[17]C. J. Horowitz, Phys. Lett. B **196**, 285 (1987).
[18]W. G. Love, K. Nakayama, and M. A. Franey, Phys. Rev. Lett. **59**, 1401 (1987).
[19]J. A. McNeil, J. Shepard, and S. J. Wallace, Phys. Rev. Lett. **50**, 1439 (1983); **50**, 1443 (1983).
[20]B. C. Clark, S. Hama, R. L. Mercer, L. Ray, and B. D. Serot, Phys. Rev. Lett. **50**, 1644 (1983).
[21]D. P. Murdock and C. J. Horowitz, Phys. Rev. C **35**, 1442 (1987).
[22]J. A. Tjon and S. J. Wallace, Phys. Rev. C **32**, 1667 (1985); **35**, 280 (1987); **32**, 267 (1985); **36**, 1085 (1987).
[23]N. Ottenstein, S. J. Wallace, and J. A. Tjon, Phys. Rev. C **38**, 2272 (1988); **38**, 2289 (1988).
[24]M. V. Hynes, A. Picklesimer, P. C. Tandy, and R. M. Thaler, Phys. Rev. C **31**, 1438 (1985).
[25]J. A. McNeil, L. Ray, and S. J. Wallace, Phys. Rev. C **27**, 2123 (1983).
[26]C. J. Horowitz and B. D. Serot, Nucl. Phys. **A368**, 503 (1981).
[27]L. Ray, Phys. Rev. C **35**, 1072 (1987).
[28]E. L. Lomon and H. Feshbach, Ann. Phys. (N.Y.) **48**, 94 (1968).
[29]E. L. Lomon, Phys. Rev. D **26**, 576 (1982).
[30]R. V. Reid, Ann. Phys. (N.Y.) **50**, 411 (1968).
[31]R. A. Arndt, L. D. Roper, R. A. Bryan, R. B. Clark, B. J. VerWest, and P. Signell, Phys. Rev. D **28**, 97 (1983); phase shift solutions SP82 and WI84 were obtained from the SAID Dialin computer program.
[32]P. Gonzalez and E. L. Lomon, Phys. Rev. D **34**, 1351 (1986).
[33]K. M. Watson, Phys. Rev. **89**, 575 (1953).
[34]L. Ray, W. R. Coker, and G. W. Hoffmann, Phys. Rev. C **18**, 2641 (1978).
[35]L. Ray, Phys. Rev. C **19**, 1855 (1979).
[36]L. Ray, G. W. Hoffmann, M. Barlett, J. McGill, J. Amann, G. Adams, G. Pauletta, M. Gazzaly, and G. S. Blanpied, Phys. Rev. C **23**, 828 (1981).
[37]In the Watson multiple scattering formalism the projectile is assumed to be distinct from the constituent nucleons in the target. For nucleon-nucleus scattering antisymmetrization is restored for the two-body operators by simply excluding the $L+S+T=$even NN partial wave states as explained in G. Takeda and K. M. Watson, Phys. Rev. **97**, 1336 (1955). The next leading three-body antisymmetrization correction is negligible except for incident energies less than the Fermi energy of the nucleus as shown in L. Ray, Phys. Rev. C **39**, 1170 (1989). Therefore, although an unsymmetrized projectile-nucleon t matrix is evaluated the procedure for restoring proper antisymmetrization is completely under control and is very accurate.
[38]K. A. Brueckner and C. A. Levinson, Phys. Rev. **97**, 1344 (1955).
[39]The problem being solved here corresponds to NN scattering where in intermediate states propagation occurs as if the two particles were in uniform nuclear matter.
[40]T. Cheon and E. F. Redish, Phys. Rev. C **39**, 331 (1989).
[41]The NN COM energy variation with momentum transfer associated with optimal factorization prescriptions was not included in $\langle t(GQ-g)t^W\rangle$ at intermediate energies since this produces small effects in proton-nucleus scattering (see Ref. 25). This energy variation was included, however, in the dominant term $\langle t\rangle$.
[42]M. Lacombe, B. Loiseau, J. M. Richard, R. Vinh Mau, J. Côté, P. Pires, and R. de Tourreil, Phys. Rev. C **21**, 861 (1980).
[43]The r-space mesh points used in solving the coupled integral equations were distributed as follows: 60 points from $r=0.03$ to 1.8 fm and 40 points from $r=1.95$ to 7.8 fm (from H. V. von Geramb). For the $^1F_3$ NN partial wave channel 10 points from $r=0.05$ to 0.5 fm, 60 points from $r=0.522$ to 1.8 fm, and 30 points from $r=2.0$ to 7.8 fm were used.
[44]M. J. Moravcsik, *The Two-Nucleon Interaction* (Clarendon, Oxford, 1963), pp. 11–18.
[45]L. G. Arnold *et al.*, Phys. Rev. C **25**, 936 (1982).
[46]R. M. Sealock *et al.*, Phys. Rev. Lett. **62**, 1350 (1989).
[47]J. J. Kelly, Phys. Rev. C **39**, 2120 (1989); J. J. Kelly, private communication.
[48]For targets such as ^{208}Pb with a large neutron excess in the surface region one might consider evaluating the NN t matrices $t^a_{pJ}(q,\rho)$ and $t^{c_0}_{pJ}(q,\rho)$ at the appropriate proton or neutron density using separate proton and neutron Fermi momenta. The resulting differences in the isovector components of the NN effective interaction from that computed assuming the isoscalar matter density as in Eq. (13) could be of interest in (p,n) charge exchange or (p,p') $\Delta T=1$ reactions on heavy nuclei.
[49]I. Sick and J. S. McCarthy, Nucl. Phys. **A150**, 631 (1970).
[50]I. Sick, J. B. Bellicard, J. M. Cavedon, B. Frois, M. Huet, P. Leconte, P. X. Ho, and S. Platchkov, Phys. Lett. **88B**, 245 (1979).
[51]H. J. Emrich, G. Fricke, G. Mallot, H. Miska, H.-G. Sieberling, J. M. Cavedon, B. Frois, and D. Goutte, Nucl. Phys. **A396**, 401c (1983).
[52]B. Frois, J. B. Bellicard, J. M. Cavedon, M. Huet, P. Leconte, P. Ludeau, A. Nakada, P. Z. Hô, and I. Sick, Phys. Rev. Lett. **38**, 152 (1977).

[53]W. Bertozzi, J. Friar, J. Heisenberg, and J. W. Negele, Phys. Lett. **41B**, 408 (1972).
[54]J. Dechargé and D. Gogny, Phys. Rev. C **21**, 1568 (1980); J. Dechargé, M. Girod, D. Gogny, and B. Grammaticos, Nucl. Phys. **A358**, 203c (1981); J. Dechargé, private communication.
[55]E. Bleszynski *et al.*, Phys. Rev. C **37**, 1527 (1988); C. A. Whitten, Jr., private communication.
[56]D. Lopiano *et al.*, private communication.
[57]G. S. Adams *et al.*, Phys. Rev. Lett. **43**, 421 (1979).
[58]R. W. Fergerson *et al.*, Phys. Rev. C **33**, 239 (1986).
[59]D. A. Hutcheon *et al.*, Nucl. Phys. **A483**, 429 (1988).
[60]G. Bruge, Saclay Report DPh-N/ME/78-1, 1978 (unpublished).
[61]O. Häusser *et al.*, Phys. Lett. B **184**, 316 (1987).
[62]B. Aas *et al.*, Nucl. Phys. **A460**, 675 (1986).
[63]N. Hintz, J. Amann, M. Barlett, D. Cook, M. Franey, K. Jones, A. Mack, G. Pauletta, B. Andrews, D. Ciskowski, L. Ping, and M. Purcell (unpublished); N. M. Hintz, University of Minnesota Summary Progress Report 1984–1987 (1987), p. 95; N. M. Hintz, University of Minnesota Progress report, 1989.
[64]G. W. Hoffmann *et al.*, Phys. Rev. C **21**, 1488 (1980).
[65]G. W. Hoffmann *et al.*, Phys. Rev. C **24**, 541 (1981).
[66]L. Ray, in *The Interaction Between Medium Energy Nucleons in Nuclei (Indiana University Cyclotron Facility, Bloomington, Indiana, 1982)* (Ref. 8), p. 121.
[67]L. Ray, G. W. Hoffmann, M. L. Barlett, and N. Ottenstein, Phys. Rev. C **37**, 224 (1988).
[68]R. J. Glauber and P. Osland, Phys. Lett. **80B**, 401 (1979).
[69]W. R. Coker and L. Ray, University of Texas report, 1989.
[70]J. W. Negele and D. Vautherin, Phys. Rev. C **5**, 1472 (1972).
[71]A general idea of the uncertainty in phenomenological real, central proton-nucleus optical potentials in the interior can be ascertained by examining the compilation in C. M. Perey and F. G. Perey, At. Data Nucl. Data Tables **13**, 293 (1974).
[72]E. van Faassen and J. A. Tjon, Phys. Rev. C **33**, 2105 (1986); **30**, 285 (1984); J. A. Tjon and E. van Faassen, Phys. Lett. **120B**, 39 (1983).
[73]T.-S. H. Lee, Phys. Rev. C **29**, 195 (1984).